FINAL SCIENTIFIC/TECHNICAL REPORT

SECA Coal-Based Systems – LGFCS

August 11, 2016

WORK PERFORMED UNDER AGREEMENT

DE-FE0012077
DUNS 78-101-6477

(period of performance Oct.1, 2013 through Mar. 31, 2016)

SUBMITTED BY

LG Fuel Cell Systems Inc.
6065 Strip Ave. NW
North Canton, OH 44720

PRINCIPAL INVESTIGATOR

Richard Goettler
330-491-4821 (phone)
330-491-4808 (fax)
richard.goettler@lgfcs.com

SUBMITTED TO

U. S. Department of Energy
National Energy Technology Laboratory

Patcharin Burke
Patcharin.Burke@netl.doe.gov

Disclaimer:

TABLE OF CONTENTS

1.0 EXECUTIVE SUMMARY

LGFCS is developing an integrated planar (IP) SOFC technology for mega-watt scale distributed power generation including the potential for use in highly efficient, economically competitive central generation power plant facilities fuel by coal synthesis gas. The overall goal of this project is to demonstrate, through analysis and testing, progress towards adequate stack life and stability in a low-cost solid-oxide fuel cell (SOFC) stack design. The emphasis of the proposed work has been the further understanding of the degradation mechanisms present within the LGFCS SOFC stack and development of the active layers to mitigate such mechanisms for achievement of a lower rate of power degradation. Performance enhancement has been achieved to support cost reduction. Testing is performed at a range of scales from single cells to ~350 kW bundles and ultimately pressurized 15kW blocks in test rigs that are representative of the product system cycle. The block is the representative fuel cell module that forms the building block for the LGFCS SOFC power system.

Major technical advances during the course of the project have been:

1. Demonstrated area specific resistance of <0.28 ohm-cm^2 in block testing that is <0.04 lower than previous baseline technology.
2. Demonstrated area specific resistance of ~0.23 ohm-cm^2 at bundle scale offering further efficiency improvement and cost reductions to early product designs.
3. Validated optimized cell print designs that will provide an additional >5% power output per substrate
4. Further advanced in-house methodologies for accelerated durability testing of anodes and cathodes to provide a means for more rapid screening and selection of active layer materials which will provide longer life of the fuel cells in service.
5. Achieved improved phase stability for a relatively new class of nickelate cathode materials. Testing to 8000 hours has validated this class of cathode compositions for escalation in testing to higher technology readiness level platforms. These cathodes can provide an additional 0.02 ohm-cm^2 lowering of area specific resistance.
6. Degradation rates achieved in testing to 2 year time frames and when combined with the lower area specific resistance technology projects to ~3 year service life while maintaining projected system performance requirements. Average ASR degradation rates of 8 mohm-cm^2/1000 hours, corresponding to power degradation rates of ~0.5%/1000 hours have been measured.
7. Insight gained from post-test analysis of long-term and accelerated tested articles has guided the selection of optimized active layer materials for the next round of durability evaluations seeking an extension in service life to more than 5-years.
8. An approach to anode protection during startup, shutdown and emergency events was developed that offers the potential to reduce the cost of the anode protection subsystem by up to 75% from initial designs.
9. Activity based cost models at high volume production rates at commercialization provide estimated average stack costs of $215/kW and average system costs of $867/kW in $201l, meeting DOE metrics.

2.0 MILESTONE STATUS

The Milestone Log shown in Table 1 represents that included in the Program Management Plan (PMP).

Table 1. Milestone Log

No.	Milestone Title/Description	Orig. Planned Completion Date	Revised Completion Date	Actual Completion Date
1	Submit Revised Project management Plan	31-Oct-13		31-Oct-13
11	Submit 4-strip DE-FE0000303 Block Test 1500 Hour Report	30-Apr-14	31-Aug-15	28-Mar-16
4	Select Active Layer Technology for Add'n Block Test	30-Jun-14		20-Jun-14
3	Submit Report for Cost Metric	30-Oct-14	27-Feb-14	18-Mar-16
10	Demonstrate Nickelate Cathodes with Phase Stability and Microstructure Design Achieving 0.02 lower ASR than LSM-based technology	30-Sep-14	30-Apr-14	30-Jun-15
5	Complete >5000 Hour Pressurized Bundle Demonstrating <0.75%/1000 Degradation	31-Oct-14		26-Nov-14
2	Submit Technical Topical Report	31-Oct-14	16-Feb-14	19-Mar-16
6	PIC ASR<0.05 Qualified for Improved Durability	30-Dec-14		31-Mar-16
7	Combined Cell Technology Demonstrating Degradation Rates Trending to 3-Yr Service Life	30-Dec-14	30-Sep-15	31-Mar-16
8	System Average 860C ASR <0.23 Demonstrated at Bundle Scale	30-Dec-14	27-Feb-15	30-Nov-15
9	Demonstrate hibernation scheme, sufficient anode redox tolerance	30-Dec-14		30-Dec-14
12	Submit 4-strip DE-FE0000303 Block Test Final Report	13-Jan-15	30-Sep-15	post-prgm, non-DOE supported
13	Complete Cell Post-test Analysis of DE-FE0000303 Block Test	9-Mar-15		30-Sep-16
14	Submit Additional Block Test >1000 Report	31-Mar-15	15-Jun-15	28-Mar-16

3.0 PROJECT DETAILS

Task 1.0 Project Management

Approach - The purpose of this task is to manage and direct the project in accordance with the Project Management Plan to meet all technical, schedule and budget objectives and requirements and ensure that project plans, results, decisions, etc. are appropriately documented and project reporting and briefing requirements are satisfied

Results and Discussion –LGFCS has participated in semi-annual technical reviews, the Annual SECA Workshop, Core Technology Reviews and SECA Program Peer Reviews. The project's performance period was originally October 2013 through March 2015. The project was granted a no-cost extension through the end of March 2016.

Task 2.0 System Costs

LGFCS utilized the Factory Cost Model developed during Phase 1 to prepare a Factory Cost Report estimating the costs for the SOFC stack at future high volume production rates. The updated stack cost estimates incorporate the demonstrated improvements in power output of the fuel cell and changes to the material compositions of the active cell layers for cost reduction. The Factory Cost Model is run with the materials set present in the metric block and for lower cost and lower ASR material sets matured sufficiently for demonstration in bundle tests run at fully representative system conditions but not deemed a priority for inclusion in block-scale tests. These lowest cost material sets to be tested at bundle scale are considered the mature, commercial sets at the time of high volume production whereas the block-scale tests incorporate the material sets for entry-into- service units. The costs are assessed on normal operating conditions achieved for the >15kW metric block test as well as peak power.

Results and Discussion –The DOE has established a manufacturing cost target of $900/kW for the coal-based power system with the associated stack cost target of <$225/kW (in $2011). To quantify

the high-volume manufacturing cost for the SOFC blocks, LGFCS has developed an extensive, activity-based manufacturing cost model. This comprehensive spreadsheet model incorporates all of the variable and fixed cost components generally associated with the manufacture of products. These cost components are calculated for each stage of SOFC block manufacturing, and then collected to provide the direct and indirect factory costs. The cost model also includes balance-of-plant equipment (BOP) as needed to comprise a 100-MW fuel cell plant. Included in the BOP equipment are turbogenerators, power electronics, controls, safe gas subsystems, and package and integration of the components. Although the cost model details are primarily focused on the smaller components leading up to the integrated stack block, the BOP equipment is factored into the cost to allow evaluation of the overall plant cost.

The Cost Model was run involving key variables with assumed cost distributions and incorporating the latest cell material sets, projected substrate sizing, and projected raw material and ceramic component specification and pricing. Monte Carlo simulations of 5000 trials were run to generate the estimates (Figure 1). The cost model estimates an average stack cost of $215.35/kW in $2011 and there is a 96.75% confidence that the average falls within ±25% of the mean (between $161.51 and 269.19/kW) for this Monte Carlo simulation of 5000 trials. The average system costs are estimated at $867.8/kW in $2011 there is a 100% confidence that the average falls within ±25% of the mean (between $650.85/kW and $1084.75/kW).

The model assumes system operation including 50% in-block reforming that facilities running at high current densities while maintaining acceptable block temperature distributions. This also serves to allow the turbogenerator to serve a larger vessel power output, supported lower turbogenerator costs. Design point operating conditions of such a system is 420mW/cm^2 and this normal operating condition was utilized in the cost estimation. Operation under these conditions has been achieved at TRL5 and entering TRL6 testing in mid-2016 under DE-FE0023337. LGFCS cell technology is meeting power degradation targets that have been set under DE-FE0012077. LGFCS is continuing to evolve its SOFC technology to achieve lower degradation, longer lifetimes (3-5 years) for early product.

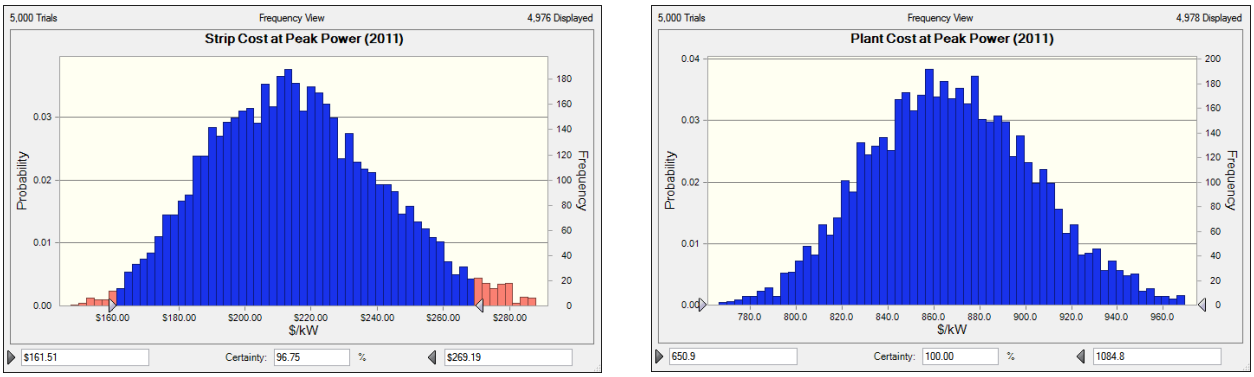

Figure 1. Monte Carlo results of high volume strip and system costs

Task 3.0 - Cell Development

Development activities have been performed on all the active layers of the LGFCS SOFC with the objective of further lowering costs and improving durability supportive of commercial system requirements.

Task 3.1 Cell Durability

The requirements for the fuel cell are based upon customer and market expectations for service life and cost. Life-cycle costs escalate if stacks replacement is too frequent so a service life of 5-years (~40,000 hours) is desired for early commercial products. The operating conditions of an SOFC system also strongly affect cost, influencing the number of stacks required to deliver power output and efficiency. LGFCS has emphasized ASR reduction to increase power output, minimizing the number of stacks and initial cost while also widening the range of ASR change permitted where the system can operate within desired conditions minimizing life-cycle costs.

One system operating scenario delivers a rated power output with degrading efficiency until a defined system ASR limit is reached based upon the system's ability to manage the stack heat generation. At the point the system is at its maximum cooling capacity the power output must be reduced to maintain the block temperature limits. Such an operation scenario is summarized graphically in 2 and assumes a system peak ASR of 0.42 ohm-cm^2. The power and stack DC efficiency is given for two stages of stack technology: (1) an initial ASR of 0.28 ohm-cm^2 and a degradation rate 8 mohm-cm^2/khrs, and (2) an initial ASR of 0.24 ohm-cm^2 and a degradation rate 5 mohm-cm^2/khrs. The 0.28 ohm-cm^2 ASR technology is the baseline at the end of this program having progressed with various cell and stack designs.

It should be noted that LGFCS is targeting current density operation greater than 450 mA/cm^2 to minimize stack costs while still delivering average lifetime DC efficiency of >60%.

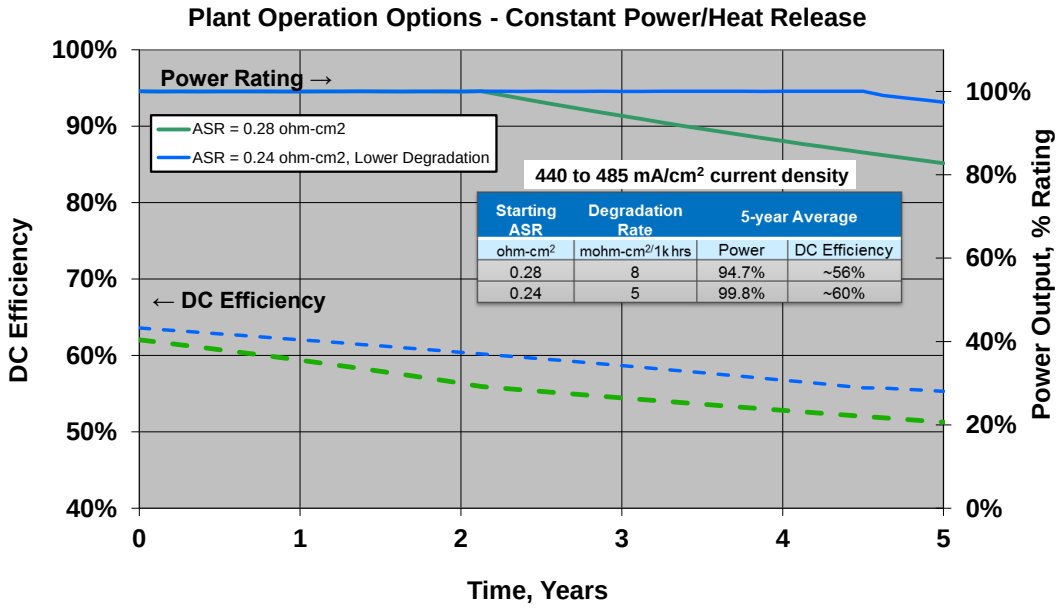

Figure 2. System power and efficiency trends with 2 stages of stack technology

Experimental Method

LGFCS relies on pressurized, full system condition testing of subscale (5-cell) and bundle (~325-440W) scale durability testing to qualify the cell materials and to validate system start-up/shutdown processes. Testing conditions include a range of stack temperatures and fuel utilizations running for a minimum of 3000 hours with some 5-cell tests of next generation cell technology surpassing 10,000 hours. A pressurized bundle test incorporating cell technology selected as a top candidate for entry-into-service systems ran for about 4000 hours and atmospheric triple-bundle tests used to pre-screen advanced cell technology for improved durability and cost reduction ran for over 16,000 hours. Testing included investigation of cell tolerance to hibernation schemes required for anode protection during emergency shutdown procedures of planned commercial systems. The impact of contaminants was also examined. Examples of these test platforms are shown in Figure 3.

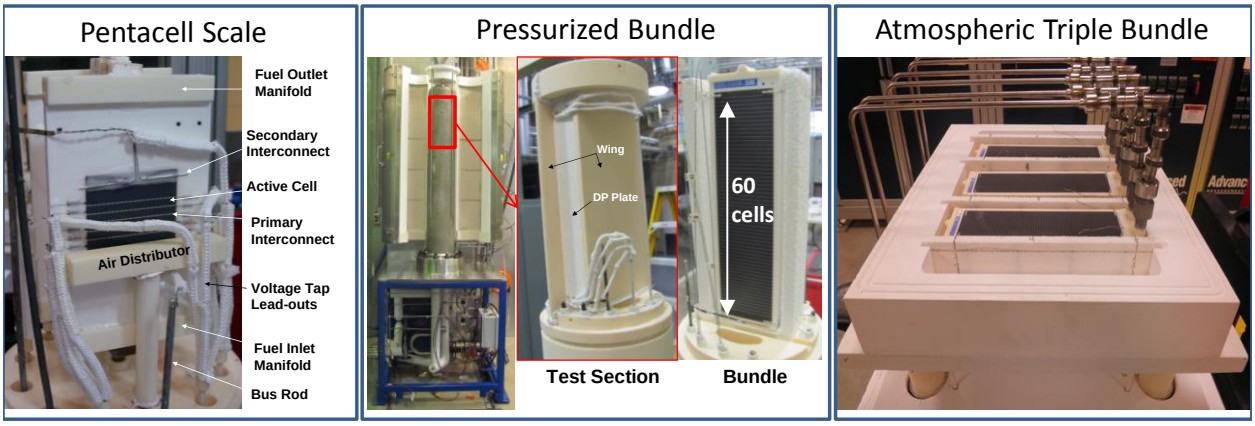

Figure 3. Subscale and bundle durability test platforms

Candidate materials were then selected for inclusion in the program supported block tests to demonstrate the ability to meet target degradation rates for a commercial product, delivering a power degradation rate of <0.75% per 1000 hours within a system representative block-scale test.

Results and Discussion

Several tests have been dedicated to long-term durability. Over the life of each test electro-impedance-spectroscopy is performed over a range of conditions every 1000 hours. The data is curve-fit using an equivalent RC circuit model to separate out the various processes within the cell which are assigned based on frequency ranges determined from parametric testing. The application of this methodology for analysis of cathode activation and the anode is shown in Figure 4. An overall average of the initial ASR and the degradation rate at 800 and 900ºC is also shown in 2 with ohmic and PIC losses included.

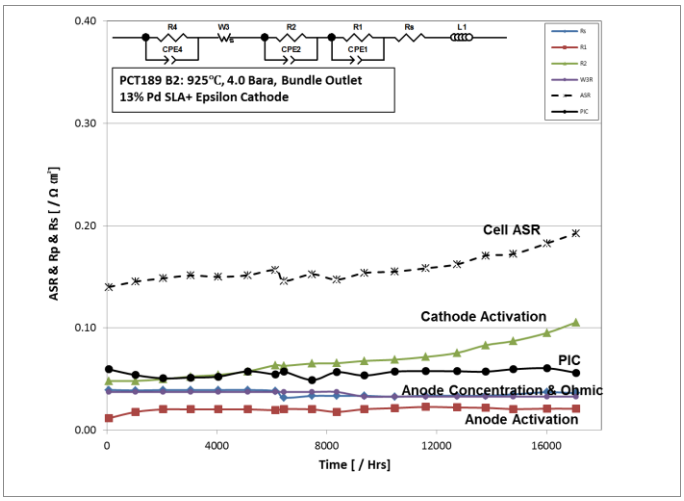

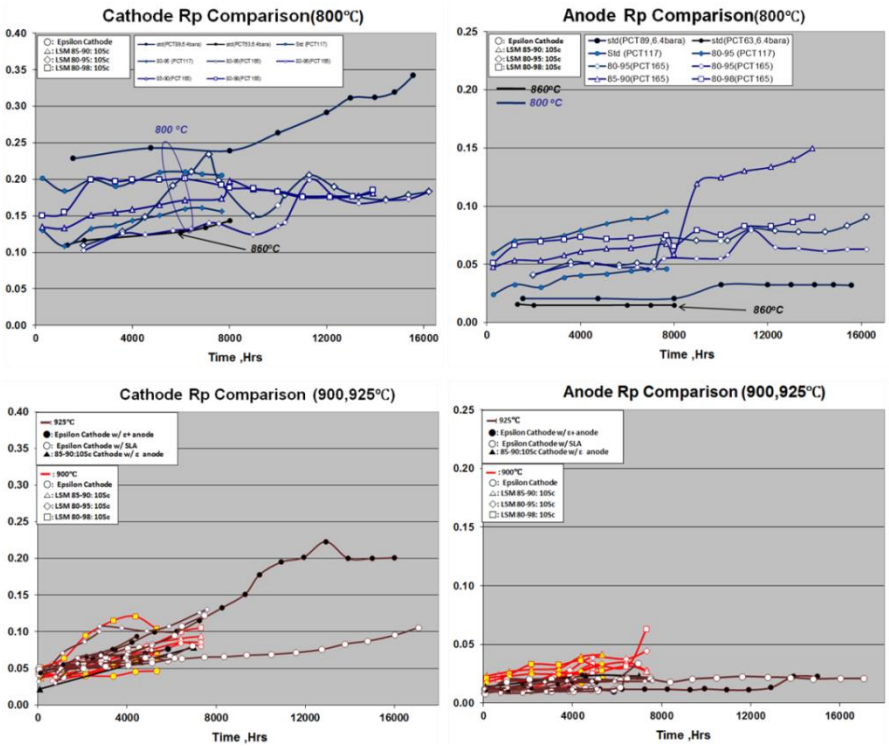

Figure 4. Equivalent circuit modelling of a long term subscale (5-cell) test data

Table 2. Summary of initial ASR and degradation rates based on RC circuit modeling of EIS data

Condition	Cathode Rp		Ohmic		Anode Rp		PIC		Combined	
	Initial Ω-cm^2	Rate μΩ-cm^2/hr	Initial Ω-cm^2	Rate μΩ-cm^2/hr	Initial Ω-cm^2	Rate μΩ-cm^2/hr	Initial Ω-cm^2	Rate μΩ-cm^2/hr	Initial Ω-cm^2	Rate μΩ-cm^2/hr
800ºC	0.11	4.7	0.07	3.6	0.04	3.4	0.07	0.8	0.337	12.5
900/925ºC	0.03	7.7	0.05	3.5	0.02	2.4	0.07	3.0	0.204	16.6

Triple bundle test: An atmospheric (1 bara) test was performed that covered the typical inlet-midpoint-outlet temperature of strips within a 5-strip block. The test was run at a system rated reformate fuel utilization of 80% and current density of 380 mA/cm^2 generally with a 2500 hour period at 530 mA/cm^2. The power and ASR plots of Figure 5 show 4 bundles as the bundle in position 3 was replaced after 5000 hours of testing because of a rig wiring related event that affected the bundle. The bundles contained the lower ASR primary interconnect composition and 2 cathode technologies (EIS1 and EIS2) alternated across the 6 substrates comprising each bundle. The combined power degradation rates for the low and mid-temperature bundle was 0.63% (ASR degradation 8.0 mohm-cm^2/khrs). Combining the high temperature bundle, the power degradation increased to 0.7% over 10,000 hours (ASR degradation 9 mohm-cm^2/khrs). Future system designs will reduce the block ΔT from the 100ºC represented by this test to ~60ºC, primarily by the incorporation of in-block reforming, and thus shift away from higher operating temperatures where degradation rates have been shown to be higher.

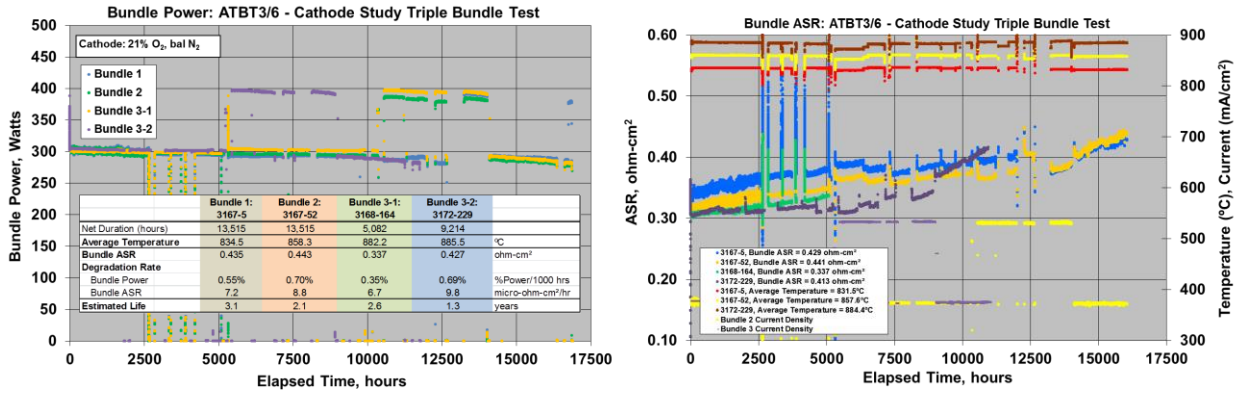

Figure 5. Power and ASR degradation observed for atmospheric triple bundle test

Pressurized bundle test: The >3500 hour milestone test was performed incorporating the EIS1 candidate cathode, a single layer anode and low ASR primary interconnect design and materials set. As shown in Figure 6 the starting ASR was ~0.25 ohm-cm^2 for the block mid-point condition (860C, 4bar). The test was run at both 380 and 530 mA/cm^2 to evaluate degradation at the higher current density range desired for lower costs. The power degradation of 0.68%/khrs met the project milestone target of <0.75%. The ASR degradation rate was 13 mohm-cm^2/khrs without any observed difference at the higher current density operation condition.

The test was also used to examine the effect of the power electronics feedback on the bundle performance. The period from about 1300 to 1650 hours included an extra ripple current (25 mA p-p at 3.8 kHz) which was the expected feedback based on power electronics testing. The period from 1650 to

2000 hours was without the ripple current. The performance during both these periods was nearly identical.

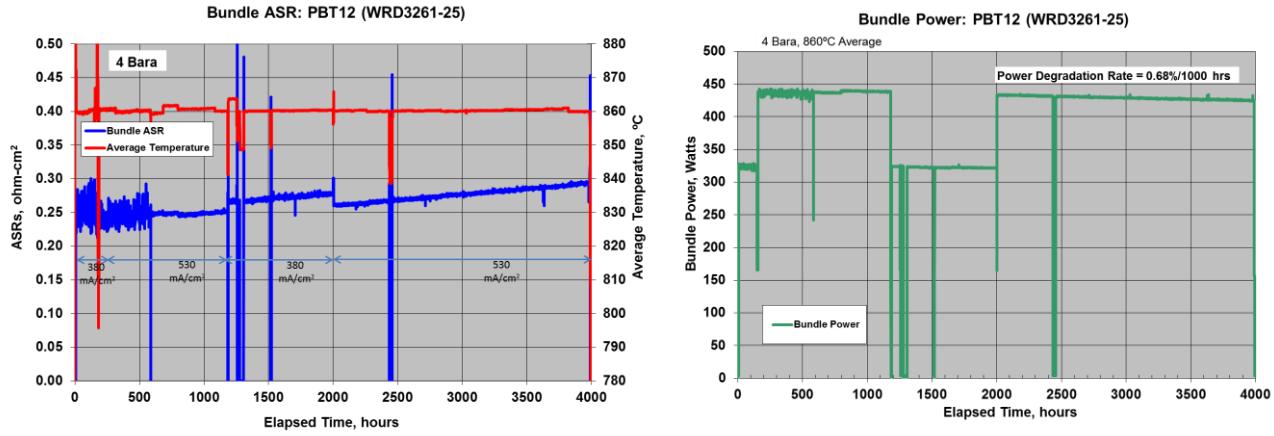

Figure 6. Durability of 4000 hour pressurized bundle test

A project milestone was demonstration of cell technology at block scale having a performance at average system operating conditions of <0.23 ohm-cm^2. This was achieved (Figure 7) with a combination of lower ASR primary interconnect design and materials and an entry-into-service (EIS) candidate cathode. Further reduction in ASR is possible with adoption of nickelate cathodes, narrower primary interconnect pitch and thinner substrate wall thicknesses.

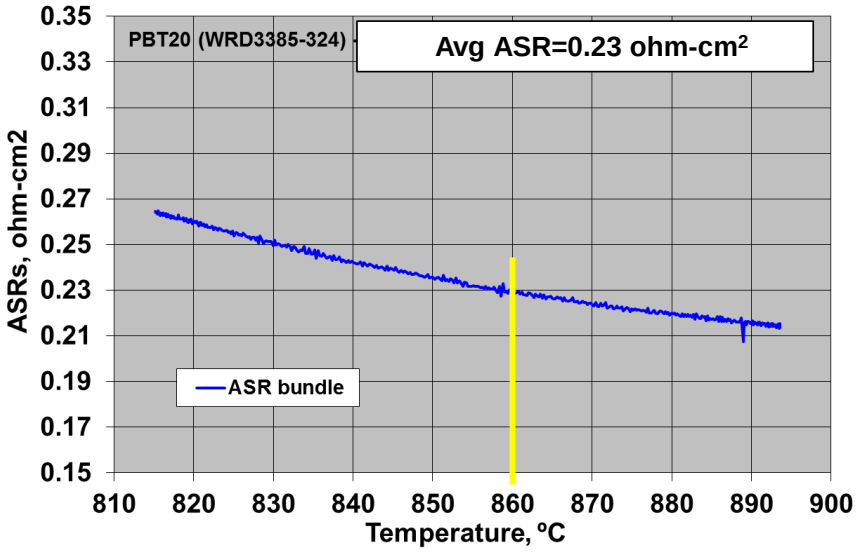

Figure 7. Lower ASR technology (pressurized bundle)

Hibernation Scheme Testing:
The conceptual hibernation schemes were based upon the premise of using a low pO_2 cathode environment to help minimize reducing gas consumption on the anode due parasitic leakage. Unfortunately these schemes tended to result in some damage as shown in Figure 8. The impedance plot shows progressive damage to both the anode and cathode, and the plot of the bundle ASR shows a significant loss of performance after each of 3 hibernation cycles.

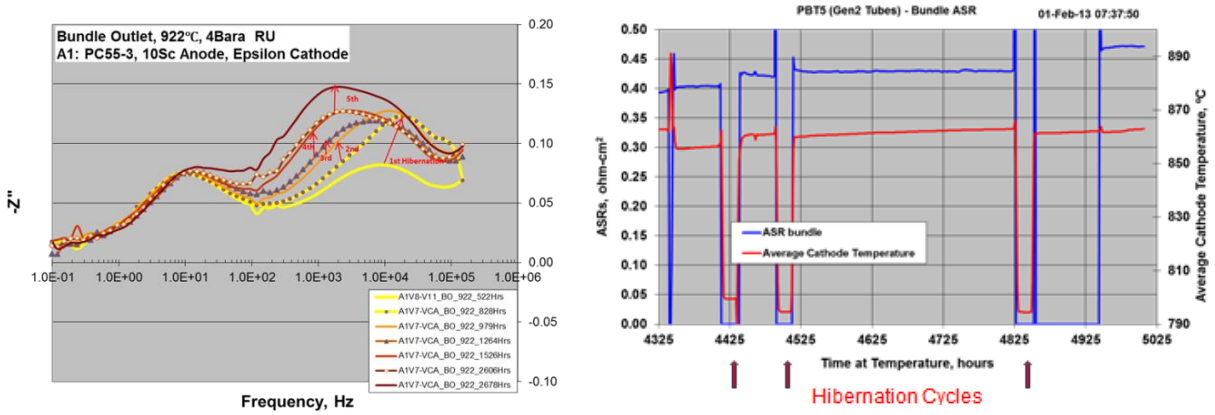

Figure 8. Increase in ASR with hibernation scheme involving lower pO_2 on cathode side

A new scheme was developed. This procedure has been performed multiple times over a 5000 hour period on a test with four 5-cell samples, showing negligible change in performance after each cycle (Figure 9).

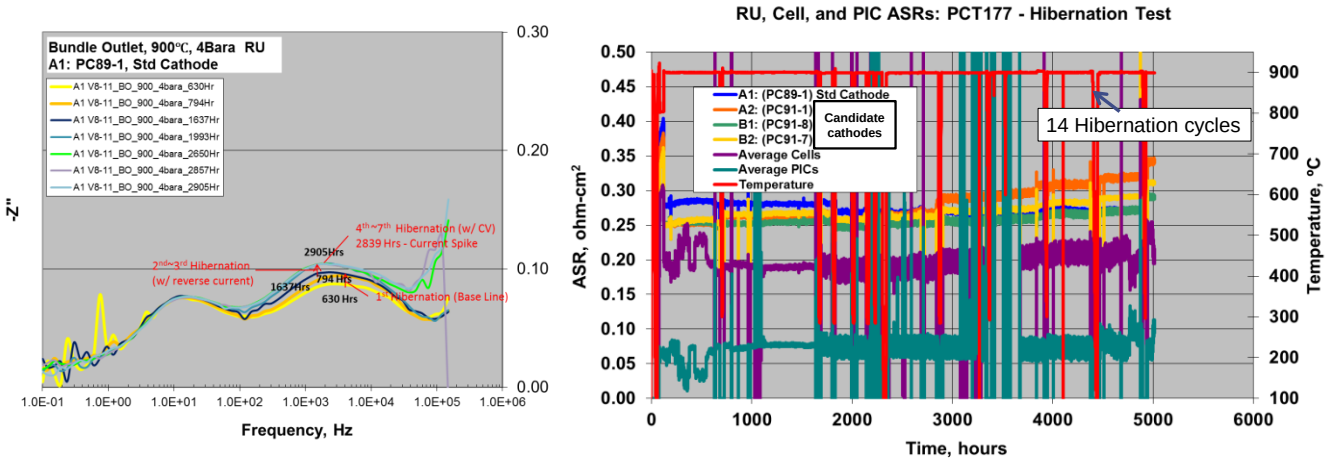

Figure 9. Improved hibernation scheme showing better ASR retention

This improved hibernation scheme was tested on a triple bundle configuration for nearly 2500 hours and 7 hibernation cycles as shown in Figure 10. The bundles are in cathode series but with independent fuel and power controls. During the hibernation cycles the bundles are electrically connected in parallel.

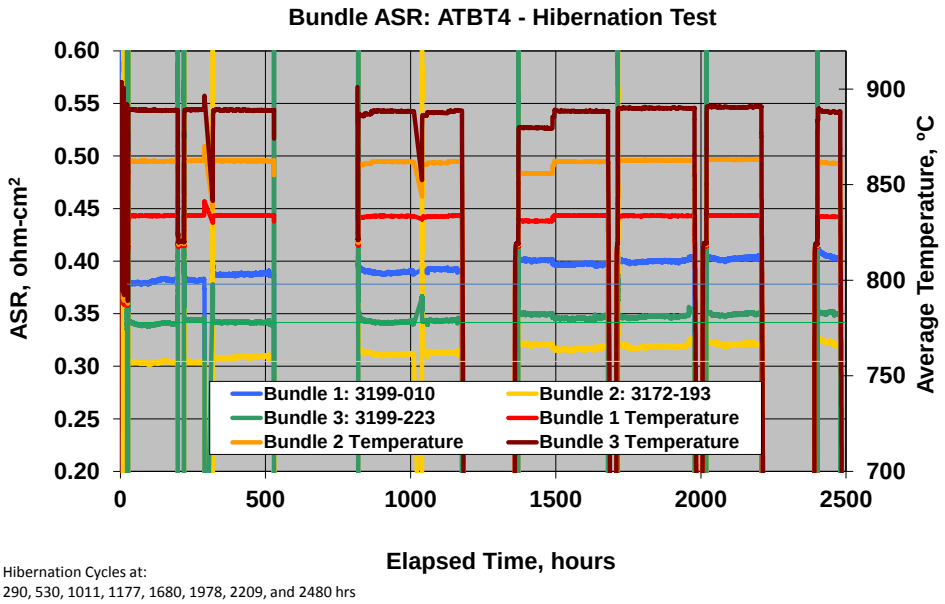

Figure 10. Durability of 3 bundles under preferred hibernation scheme

The degradation rates of the bundles are shown in 3 below. The rates were highest for the lowest operating temperature bundle, and lowest for the highest operating temperature bundle. The overall rates, however, are as expected for this period of operation, and may be more related to standard operation than due to the hibernation cycles. There has been little change in the rate of degradation over the last 3 cycles. This provides further validation of a scheme for anode protection of system level tests and future product configuration.

Table 3. Summary of degradation rates for triple bundle hibernation test

Time =	2464 hours	**Bundle 1: 3199-010**	**Bundle 2: 3172-193**	**Bundle 3: 3199-223**	
Average Temperature		833.2	861.3	888.1	ºC
Bundle ASR		0.404	0.322	0.350	ohm-cm²
Bundle Degradation Rate		10.2	8.1	5.1	micro-ohm-cm²/hr

Conclusions –Long-term atmospheric pressure bundle testing has shown ASR degradation rates in the 8 mohm-cm^2/khr range for test temperatures under 900C. Combining of that degradation rate with the lower ASR technology demonstrated at bundle scale, and for which further reduction is possible through cell and stack design changes (no different active cell materials) provides confidence that the technology is trending towards an initial service life of at least 3 years. Risks still exist as a higher current density is desired (~500 mA/cm^2), whereas most of the durability database is at 500 mA/cm^2, and system level contaminants must be minimized to avoid accelerated degradation.

Task 3.2 Primary Interconnect (PIC) Development

Experimental Method - LGFCS has optimized previous cermet via interconnect design and materials to achieve a lower cost per kW at a given fuel cell DC efficiency and to extend its durability range. Optimizations included modifying the printed features of the via for ASR reduction and adding a new functional/barrier layer for mitigating a degradation mechanism caused by material inter-diffusion. A study of reducing the PIC pitch dimension was performed to increase the active cell area by adding extra cells and thus increasing total power output per tube to reduce stack cost per kW. Investigations also covered ceramic interconnect materials and designs for further cost reduction and potential long-term durability advantages over that provided by the cermet design.

Results and Discussion

PIC printing pattern change: One of the key activities was to continue to modify the PIC printing pattern and via materials for further ASR reduction and to implement this design to the full tube and bundle level. The objective was to increase via material conductivity while keeping the same cost and to change the printing pattern for improved current flow while avoiding a significant increase to the printed PIC area.

A batch of full-sized substrates was processed using modified PIC printing pattern and higher conductive via material. Standard printed substrate quality assurance tests (1 bar, reformate) were performed to compare to baseline design and materials. Figure 11 shows the ASR (average of 5 tubes) for the modified PIC printing pattern and via materials ("TRT100") is about 0.29 ohm-cm^2 at 860^{o}C, which is about 0.05 ohm-cm^2 reduction compared to baseline technology. Since 0.05 ohm-cm^2 ASR reduction is the combination of PIC printing pattern and the via material conductivity improvement, more detailed ASR separation was conducted based on subscale test articles (5-cells) testing results. Approximately 73% of the 0.05 ohm-cm^2 reduction was attributed to the 50% increase in the conductivity of the via material and 27% from the change in the print pattern. An extreme case of PIC redesign eliminating vias in favor of a complete strip PIC pattern can offer an additional ~0.03 ohm-cm^2 reduction in PIC ASR, but material costs would be increased.

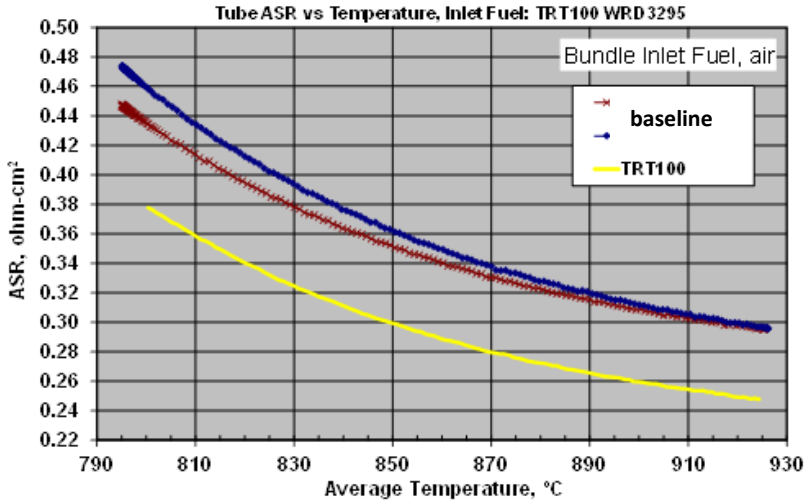

Figure 11. Tube ASR temperature sweep of modified PIC design and via materials vs. epsilon baseline

PIC pitch change for further ASR reduction: The PIC-cell pitch was redesigned in order to increase effective cell area and power output per tube for cost reduction. Ohmic resistance models of the LGFCS series connected design show an optimization in the power per tube depending on the number of cells and the length/pitch of the PIC for a set tube length (Figure 12). A new PIC-Cell pitch, 0.95 mm versus the baseline 1.1 mm was selected as the first step in reducing the pitch and assessing printing issues and ASR and power benefits. The new cell pitch represents up to 6% increase in effective cell area. The model calculation predict a decrease in the ASR of the PIC by 10% and up to ~6% power output increases for full tubes and bundles.

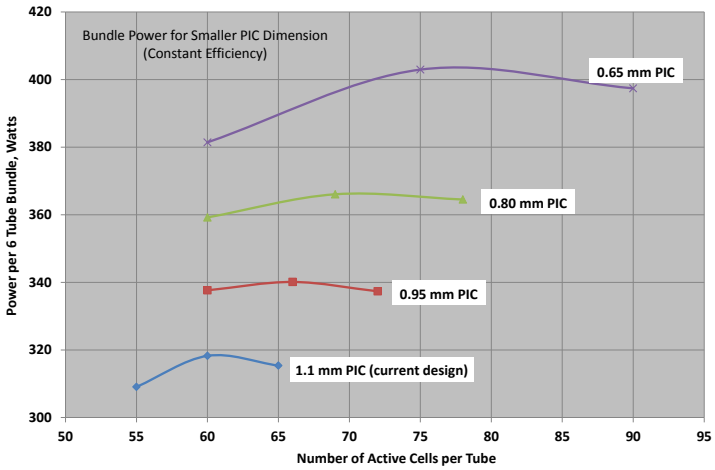

Figure 12. Estimated bundle power output vs. number of active cells per tube and PIC dimension

The 0.95mm PIC pitch was first tested with subscale cells (5 cells). Statistical data analysis of the primary interconnect ASR values (P-value 0.045) with and without the PIC redesign based on multiple subscale cell test results (Figure 13) show a reduction in ASR of 0.01 ohm-cm^2 both at start and after 1000 hours of testing. The main benefit of the short pitch the ability to print more cells per substrate.

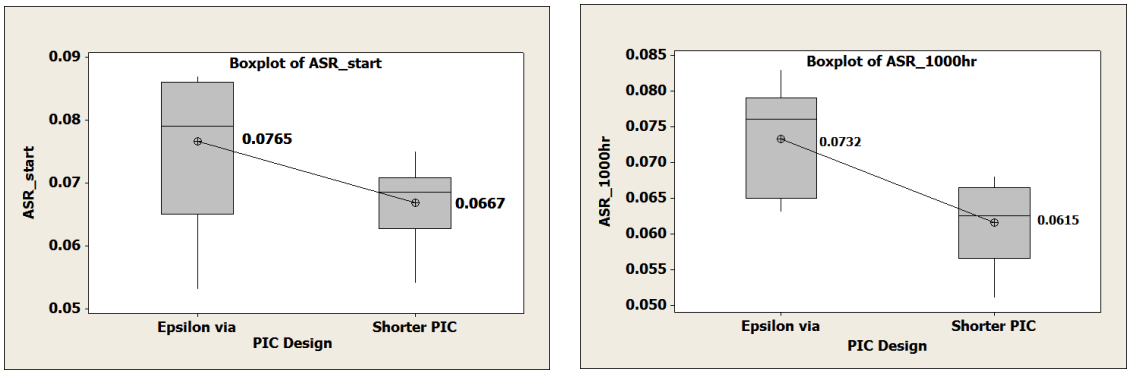

Figure 13. PIC ASR Data analysis: Epsilon via design vs. shorter PIC design (900^{o}C, reformate fuel, ambient air, 1 bara)

The shorter PIC pitch design was also demonstrated with printing of full size substrates. No printing issues were encountered. Tube ASR temperature sweep shows 0.013 ohm-cm^2 ASR reduction (Figure 14) compared to standard PIC pitch. Since the only difference is PIC pitch, we can attribute the ASR reduction to PIC pitch.

The print pattern was 63-cells versus the normal 60-cells. Substrate power increased 5.8% from 51.9 W to 54.9W due to the combination of PIC ASR reduction and cell effective area change. The ASR reduction for shorter PIC is consistent between full tube and subscale cell tests.

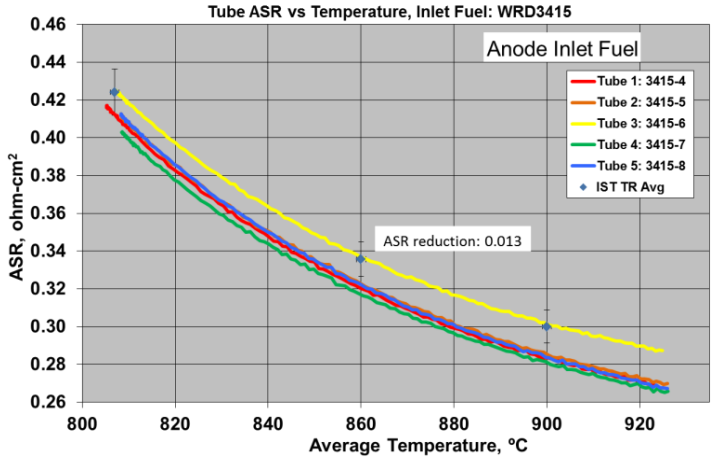

Figure 14. ASR temperature sweep of full substrates, 0.95 mm PIC pitch (bundle inlet fuel, 1 bara)

PIC materials change for improved performance and long term durability: To further mitigate the inter-diffusion degradation mechanism at the PIC, an optimized barrier design and materials are being developed. Candidate materials were screened and selected based on conductivity under different pO_2, controlled porosity, CTE, and strength.

Material modification of the chemical barrier layer was conducted to improve the mechanical integrity of the layer and minimize pathways for materials migration across layer interfaces. The coupon evaluation confirmed that the modified chemical barrier has a more favorable coefficient of thermal expansion and uniform microstructure was confirmed for printed subscale test articles. After 1000 hours of testing (Figure 15) the modified and baseline cells show a stable PIC ASR. Longer tests combined with post-test analysis is needed to determine degree of the reduction in materials migration achieved with the modified barrier.

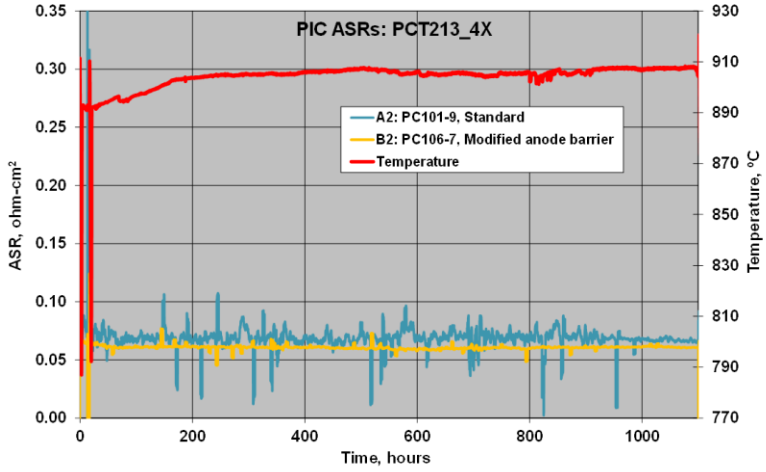

Figure 15. PIC ASR durability of subscale cells with modified anode-side barrier evaluate barrier

Use of a cathode-side barrier layer is being investigated for improved PIC long term durability. Three compositions (A, B, and C) were initially evaluated. Subscale cell testing out to 1600 hours showed that cells with modified cathode-side barrier layer have slightly lower ASR (~0.06 ohm-cm^2 vs. 0.07 ohm-cm^2) with no degradation. Post-test analysis indicated barrier layer material A exhibited significant interaction with adjacent cell materials. Barrier layer B has a favorable microstructure/density and achieved a reduction in materials migration based on EDS analysis, and was thus selected for more thorough evaluation. Long-term durability testing of a total of 7 test articles with cathode-side barrier layer B accumulated about 6,000 hours of operation at the high current density, 530mA/cm^2 and covering the system operation temperature range from 820^{o}C and 900^{o}C (Figure 16). These test articles incorporated new primary interconnect designs and materials for enhanced durability with the objective of generating the statistical database for starting ASR and long term durability of the PIC. PIC ASR average of ~0.05 ohm-cm^2 (meeting one of the program's key technical milestones) was achieved with no noticeable degradation rate in testing out to 6,000 hours. Average repeat unit (one cell plus one PIC) ASR degradation rate is 0.0043 ohm-cm^2/khrs at 900^{o}C, and 0.007 ohm-cm^2/1,000 hrs at 820^{o}C at this high current density.

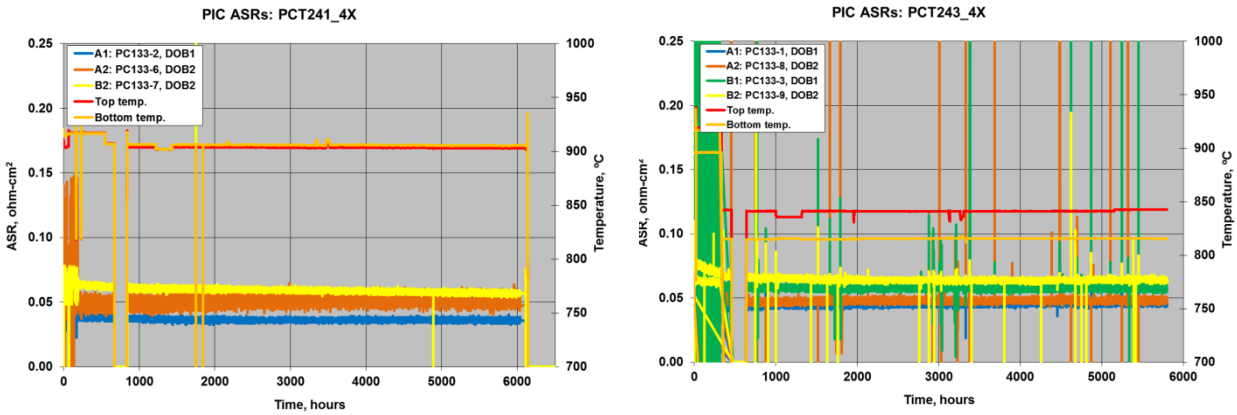

Figure 16. Long term durability of total 8 test articles for advanced PIC (Bundle inlet fuel, 1 bara)

PIC material change for lower parasitic loss: The LGFCS integrated planar SOFC design exhibits parasitic/leakage losses, but having a minor impact on efficiency. Approaches were examined for reducing the level of the parasitics. Testing has shown that ~60% of the parasitics arise from the PIC area and 40% from the active area. As shown in Figure 17, through changes in the compositions of some of the layers in PIC area TRT73 printed tubes 1 through 5) the parasitic loss was reduced. We have seen an effect on parasitic reduction of the active cell area through improvement in electrolyte quality (TRT80 data point) – more data is required to confirm trends over several lots of pilot production tubes.

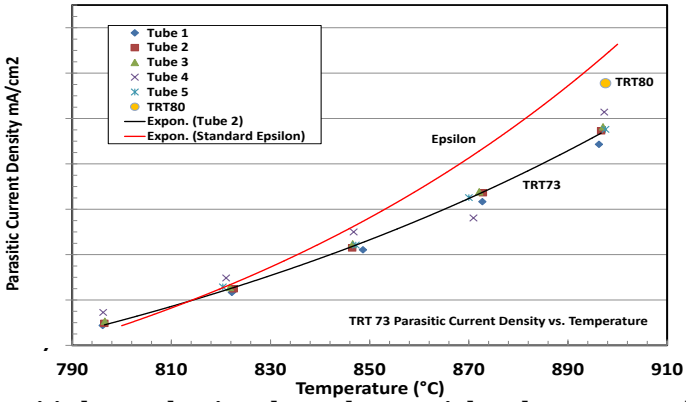

Figure 17. PIC parasitic loss reduction through material and process modification

*Ceramic interconnect:*A ceramic based primary interconnect (CIC) is LGFCS's long term objective for mature products. Bi-layered ceramic interconnect design was selected, and both air-side and fuel-side materials were evaluated. Based on previous investigation, the technical challenge has been achieving a material that meets the material stability requirements under wider pO_2 range, which could benefit bi-layered interconnect implementation to the full tubes since the pO_2 at interface of bi-layered interconnect needs to be controlled to ensure long term stability of ceramic interconnects, and that can be adequately densified in a constrained sintering condition (as printed layer on the LGFCS substrate). Figure 18 summarizes the conductivity trends for a favored air-side and fuel side composition. It can be seen that the air-side material keeps high enough conductivity, between 25 S/cm and 2.5 S/cm, from ambient air to log(pO_2) of -19, and fuel-side material shows increased conductivity at log(pO_2) of -19 and leveled off at ~2.5 S/cm after 30 hours of reduction. Based on ohmic resistance PIC modeling, the air and fuel side materials should have conductivities ≥ 1 S/cm to achieve the target PIC ASR; both air-side and fuel-side materials meet minimum requirements in their respective environments.

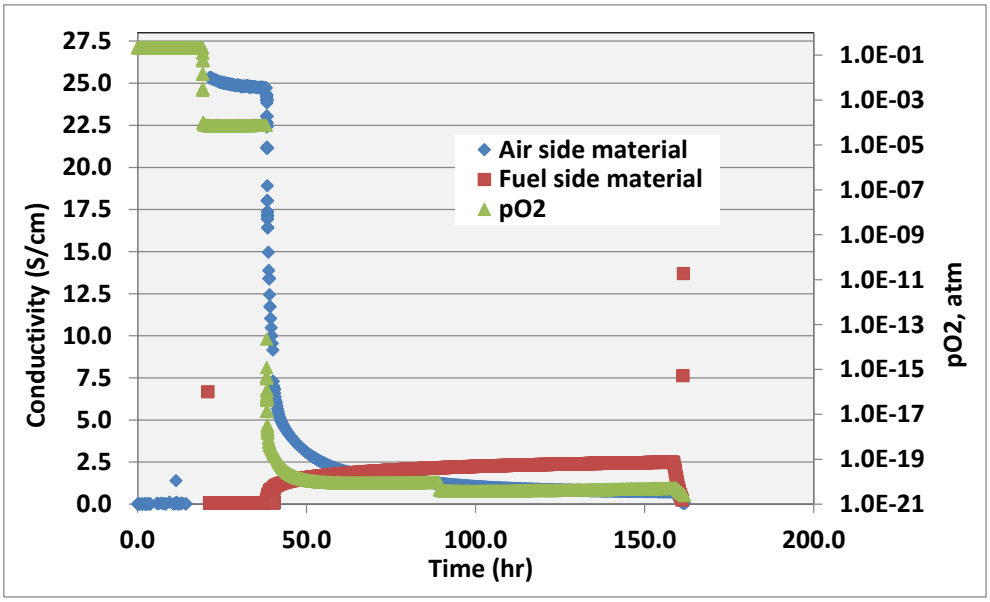

Figure 18. Conductivity of an air & fuel-side material for bi-layer ceramic interconnects

Also both air-side and fuel-side materials show excellent sinterability in pellet/bar form at normal cell processing temperature range, benefiting from sintering aids. Subsequent constrained sintering experiments by screen-printing air-side and fuel-side ceramic interconnect on top of MgO-$MgAl_2O_4$ (MMA) substrate coupons were then performed. Two different materials/compositions were selected for both air-side and fuel-side interconnect and fired at normal cell processing temperatures. All coupons show dense microstructure with low porosity (Figure 19 for fuel-side materials film coupons and Figure 20 for air-side materials film coupons).

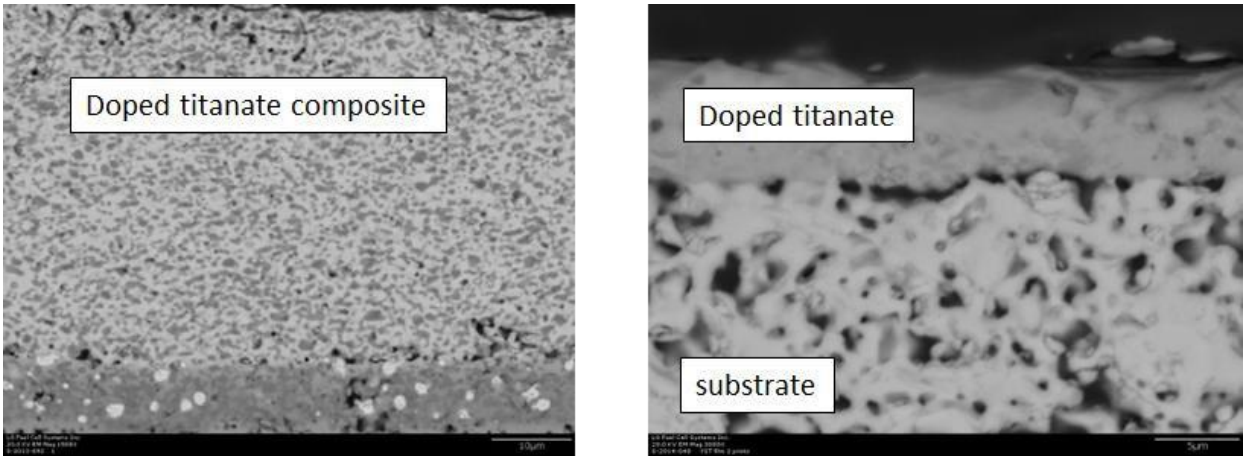

Figure 19. High degree of densification for anode-side interconnect materials

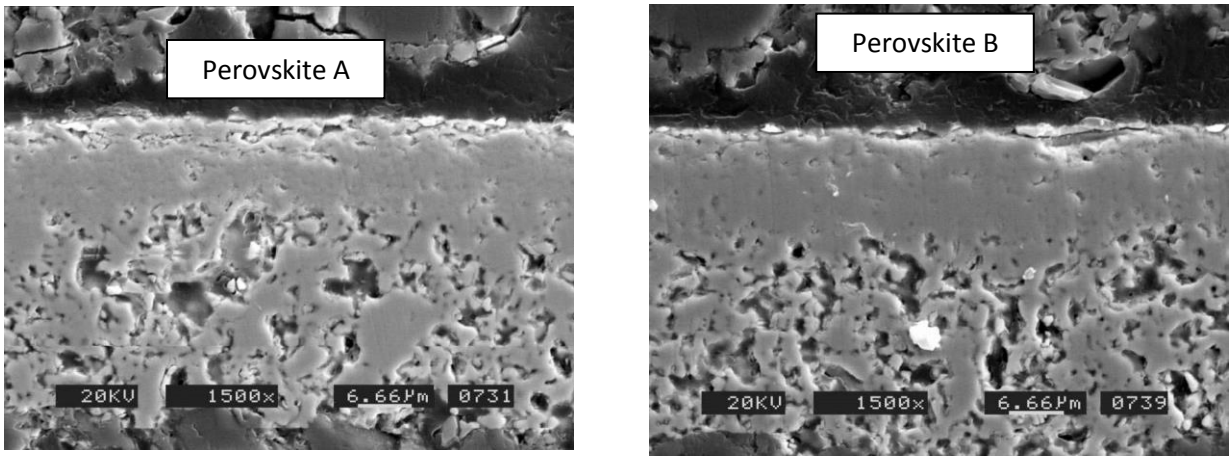

Figure 20. High degree of densification for air-side interconnect materials

Based on the densification results a fuel side layer and air-side layer were selected for electrochemical performance evaluation of a ceramic bi-layer interconnect in subscale cell test. Cells passed leakage tests confirming that the bi-layer CIC provides comparable gas tightness as the current epsilon PIC designs and sufficient densification of the CIC layers. However, the CIC showed higher initial ASR, ~3.5 ohm-cm^2 (Figure 21) with slow improvement over time. Upon switching the fuel from reformate fuel to H_2, the ASR reduced by 50% to 1.2 ohm-cm^2 and continued to show slow improvement. An increase in the temperature to 950^oC provided a slight further reduction in ASR.

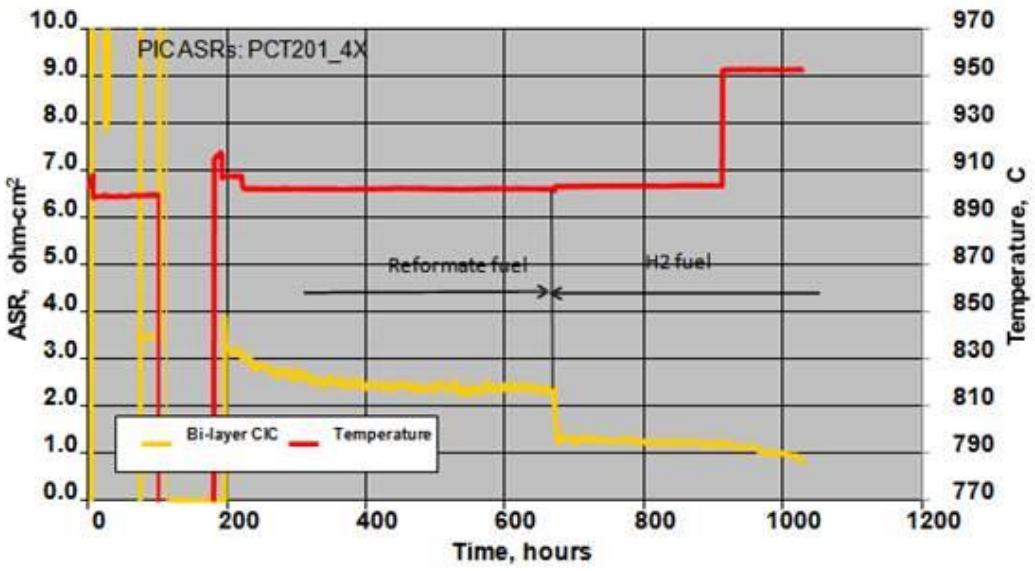

Figure 21. Bilayer CIC ASR in 5-Cell test article in ambient test rig

The CIC shows higher than expected ASR based on the model and conductivity data of bilayer ceramic interconnect measured from coupons. Materials interaction studies were initiated involving mixtures of the CIC material with fuel cell materials in adjacent layers. The three key tests are: 1) fuel-side CIC with air-side CIC, 2) Fuel-side CIC with YSZ, and 3) fuel-side CIC with NiO. For each sample, two powders were mixed with 50/50 weight ratio and pellets were made, and then fired at normal cell processing temperatures. The XRD results are shown in Figure 22. The fuel-side CIC showed no reaction with YSZ but unidentified XRD peaks were observed in mixtures with NiO. Fuel-side and air-side CIC materials have the same structure and therefore the XRD peaks generally overlapped making it difficult to ascertain the degree of reactivity.

Post-test analysis of the Figure 22 cell showed no indication of major reaction between the air and fuel side CIC materials. Some printing alignment issues were observed that resulted in the air- side material have some exposure to the fuel environment – this is deemed the primary cause of the high ASR. Future effort of bilayer CIC development will focus on printing pattern redesign and design of individual layer thickness to optimize pO_2 across the bilayer to insure adequate electrical conductivity for the various materials.

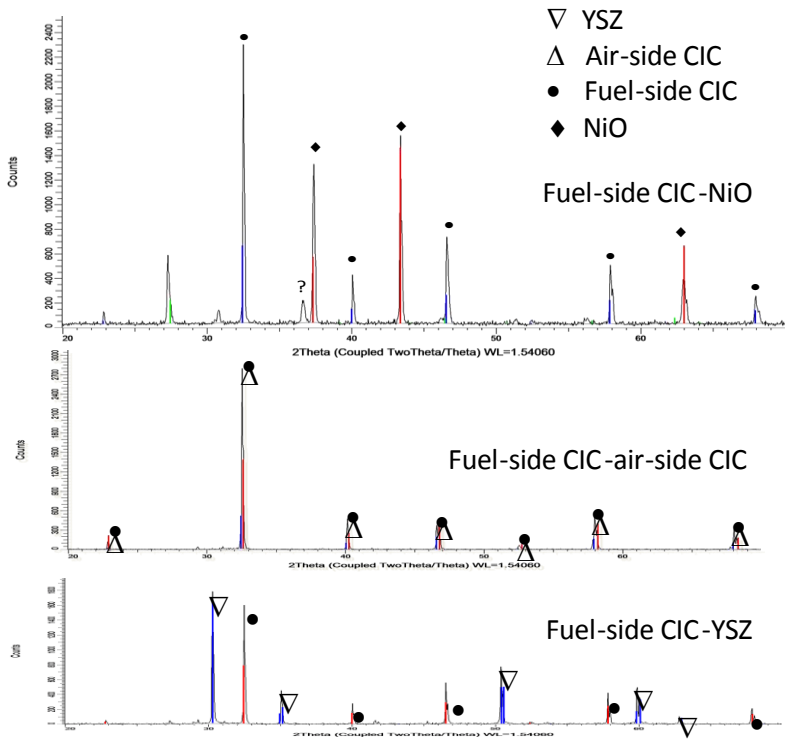

Figure 22. XRD results of pellets

Conclusion – The ASR of the primary interconnect region has been improved to 0.05 ohm-cm^2 through a design change of the via print pattern and a change to a higher conductivity via. Ohmic resistance degradation of the interconnect is not recorded in testing to 16k hours, however post-test analysis has consistently shown a degradation mechanism of some materials migration across the phases present at the PIC region, and so improvements are necessary to expect stable performance in longer-testing. Development of enhanced barrier layers at the anode and cathode sides of the PIC are showing promise and tests are continuing for further validation of long-term functionality. Constrained sintering/densification has been achieved for candidate ceramic primary interconnect materials. Further work is needed to optimize the materials and designs of the bilayer interconnect to achieve lower ASR.

Task 3.3 - Anode Development

LGFCS validated the long-term durability of its single-layer anode technology and optimized its composition, structure and processing to provide specifications for full-scale manufacturing. Such work involved defining the optimum substrate thermal expansion for adequate anode conductance while maintaining a high manufacturing yield and avoiding electrolyte cracking caused by CTE differences between the anode and the substrate. Improvements in the redox tolerance of the anode was pursued with the nearer-term objective of surviving system emergency shutdown/hibernation scenarios and with the longer-term objective of simplifying and/or eliminating the anode protection gas system in future commercial SOFC power generation systems. Methodology of anode accelerated testing was developed to facilitate materials screening.

Result and Discussion

Redox tolerant anode: A redox tolerant anode is a long term objective to protect anode when exposed to high pO2 environment during fuel cell stack emergency shutdown (ESD). Preliminary redox cycle tests confirmed that the baseline bilayer anode is able to tolerate about 5-6 redox cycles (at 900C) without causing significant damage to anode. Whereas early redox trials for single layer anodes using subscale cell test did not demonstrated comparable redox capability, showing only 2 or 3 redox cycle capability. For the initial stage of development, we have conducted preliminary redox test to understand the effect of parameters on redox tolerance for single layer anode design, such as thickness and additives. Redox screening of the single layer anodes also utilized measured changes in conductance in anode side. For anode films with initially lower conductance (~0.25S), ASR and conductance changes appear more significant. Besides the electrode thickness effect on redox, LGFCS has also investigated the effect of dopants/second phases to control the CTE and microstructure, such as porosity and metal distribution, on redox tolerance of the single layer anodes. The microstructure change could be achieved by very small amount of doping as shown in Figure 23. Such dopants had a minor affect cell ASR and anode side conductivity.

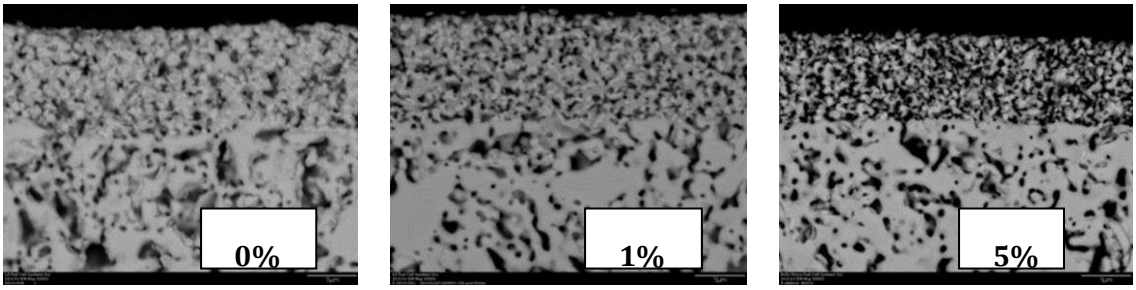

Figure 23. Microstructure, porosity of single layer anode with different doping levels

Following the initial redox study, three technical approaches were identified to develop redox tolerant anodes:

1) control particle size of ionic phase,
2) various additives
3) bi-layer structure with both composition and porosity of gradient.

Various pellet coupons were tested and evaluated under selected redox cycle conditions. After fabricating pellets with different composition, 5 redox cycles were conducted to these pellets at 900C. Redox cycles consisted of N_2 purge, air introduction to test furnace for 3hrs, then N_2 purge again, and finally reduction of the anode using fuel at 900^{o}C and 1bar. After redox cycles, pellet dimension and structural change,

including cracks, were observed. Figure 24 shows the as-fabricated and redoxed anode (5 cycles) pellets: baseline vs. anode compositions with controlled microstructure/particle size. Seven different anode compositions were designed using the powders with different particle size and the combination. Compared to the baseline sample (test #0), all pellets made from controlled ionic phase show less dimensional change after redox cycle and better mechanical integrity. Based on pellets redox results, test sample No. 1 shows least dimensional change and was selected for further evaluation. Slight changes in the NiO ratio to ionic phase didn't provide noticeable benefit on anode redox tolerance.

#	NiO	YSZ	Porosity, %
0	standard	baseline	1.24
1	standard	Modified A	3.58
2	standard	Modified B	3.56
3	standard	Modified C	1.53
4	standard	Modified D	1.28
5	standard	Modified E	1.03
6	standard	Modified F	1.30
7	standard	Modified G	1.68

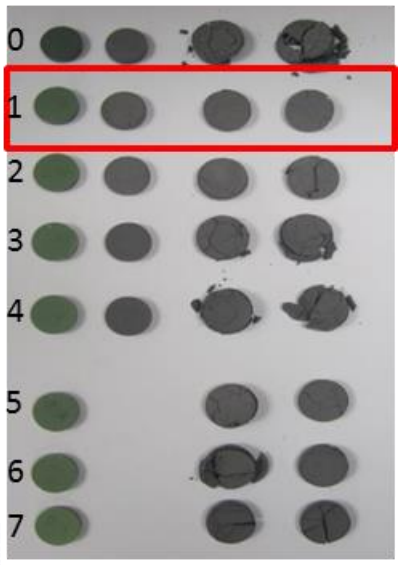

Figure 24. Pellets before/after 5 redox cycle test for ionic phase optimization approach.

Three different materials were chosen as additives to improve anode redox tolerance. After 5 redox cycles, the baseline pellet (Figure 25A) shows severe delamination and cracks. Additive A with 0.5% only shows a slight improvement based on mechanical integrity. Additive B, with addition level from 2 to 10%, shows significant improvement in anode redox tolerant - no cracks and delamination were observed (Figure 25B). The third additive (C), achieving a different Ni cermet system, was not as effective in improving redox tolerance. Additives B and C were chosen for further development of this approach.

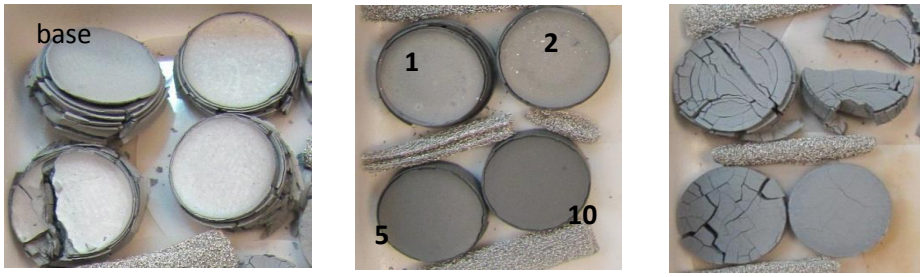

A) Additive A **B) Additive B** **C) Additive C**

Figure 25. Pellets after 5 redox cycle test for various additive approaches.

Under the bi-layer electrode design, porosity and composition of each layer was varied. Film coupon tests were required for evaluating the bilayer concepts. Candidate layers were screen printed onto substrates and conductance was measured upon reduction at 900°C and after repeated redox cycles (5 cycles). Figure 26 shows conductance change after redox cycles for 4 candidates of bi-layer coupons. Bilayer approaches 1 and 2 provided improved conductance after 5 redox cycles, so they were selected these conditions for further development.

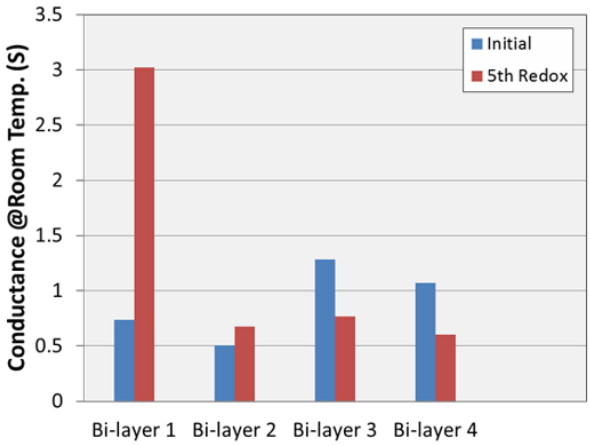

Figure 26. Conductance of test coupons before and after 5 redox cycles for bi-layer approach.

Subscale cell evaluation of redox tolerance for the various anode materials and designs selected from each approach was performed. Single cell rather than 5-cell architecture was chosen for subscale cell since the print pattern is designed to provide anode conductance measurements during testing. After initial cell performance check, redox cycles were conducted . Figure 27 shows cell ASR change with redox cycles for different single layer anode compositions and approaches. Initial single layer anode compositions could only tolerate 2 or 3 redox cycles before the cell ASR increased over 0.4 ohm-cm^2. After modification, selected single layers showed similar redox behavior as the epsilon bi-layer anode, with an ability to tolerate 4-5 cycles without a significant increase in ASR.

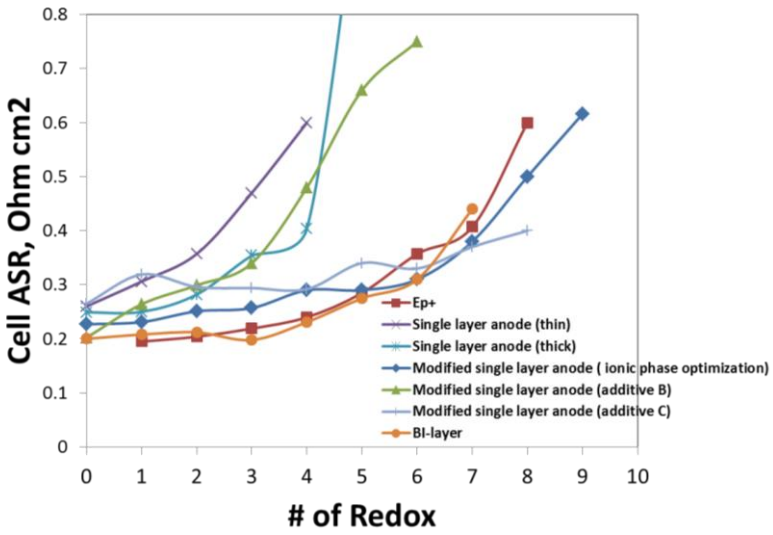

Figure 27. Cell durability with redox cycles for different anode compositions.

During redox cycles, anode side conductance was measured and its effect on cell ASR was analyzed (Fig. 28). With an increasing number of redox cycles, anode conductance decreases and the resulting ASR change matched well with the predictions from LGFCS electrochemical cell models. Cell ASR (Rp) and ohmic resistance increased slowly with decreasing anode conductance, but then increased quickly once the anode conductance fell below 0.3 S. A high initial anode conductance is preferred to achieve better redox tolerance. Anode porosity control and microstructure stability are critical. From the redox cycle testing with different anode compositions and designs, LGFCS demonstrated the technical approaches to improve anode redox tolerance. A degree of redox tolerance offers options to simplify anode protection system and reduce the cost for commercial fuel cell systems.

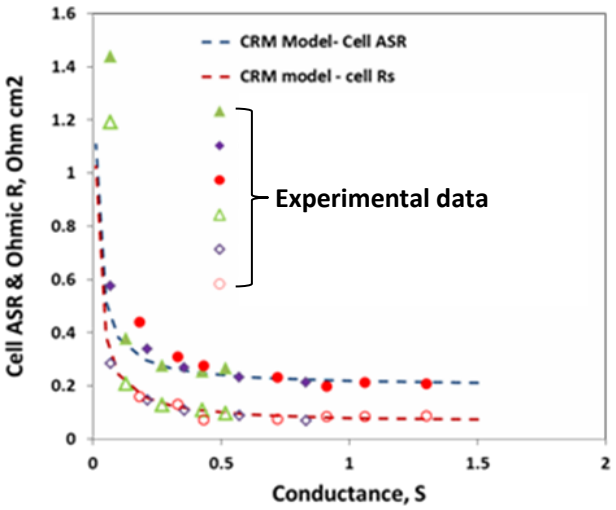

Figure 28. Cell ASR and ohmic resistance vs. anode conductance

Durability database and enhancement: Post-test analysis of traditional bi-layer active anode plus anode current collector (ACC) has revealed metal phase coarsening and migration near the anode and ACC interface, especially at higher operating temperatures and fuel utilization conditions. Single layer anodes to eliminate the anode and ACC interface was selected as the next generation anode technology. A key activity during this project period was to evaluate the long term durability of single layer anodes. Testing of single layer anodes has surpassed 17,000 hours under aggressive test conditions of bundle outlet fuel and 925C and 4 bar (Figure 29). Two penta cells (5 cells in series) with single layer anode have showed very stable repeat unit (RU) ASR with degradation rate of 0.003 ohm cm^2/ 1000hrs.

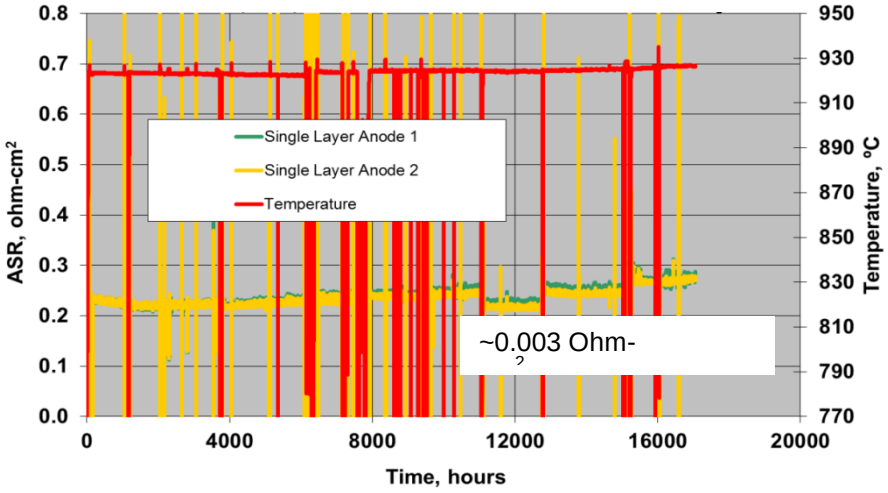

Figure 29. RU ASR durability of single layer anode cells

Figure 30 shows a single layer anode microstructure following 10,000 hours of testing under aggressive bundle outlet and 925C conditions. Coarsening is observed and some metal accumulation is present in the region near the electrolyte, nevertheless this achieved a low anodic degradation rate, and at a temperature approximately 30C higher than planned peak operating temperature of product.

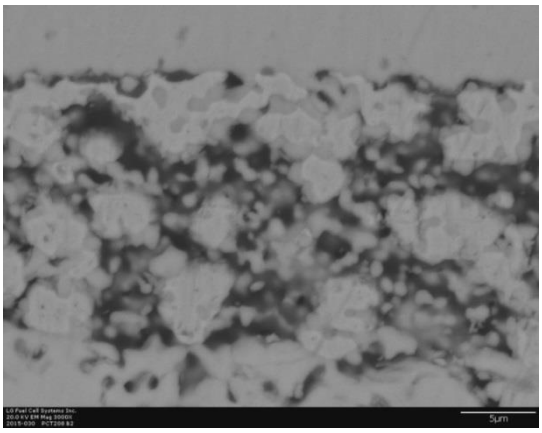

Figure 30. Single layer anode (Type II) microstructure after 10,000 hr testing

Accelerated anode testing: LGFCS developed accelerated testing protocols to evaluate different anode compositions for EIS technology since it takes a long testing period under normal operating conditions (>6,000 hrs) to show difference between epsilon and single layer anodes. Two accelerated tests (Figure 31) at 90% fuel utilization and 925^{o}C were conducted to compare epsilon and single layer anodes. Both tests exhibited similar trends. In first test (a), the epsilon bi-layer anode showed higher degradation rate, 0.08 ohm-cm^2/1000 hrs vs. 0.037 ohm-cm^2/1000 hrs for the single layer anode. For the repeat test (b), the performance at normal operating test conditions (900C, bundle inlet fuel) was compared before and after accelerated testing. The single layer anode shows almost no ASR change as a result of the ~1000 hours of operation under the harsh, accelerated testing conditions. The baseline bi-layer anode ASR increased 0.02 ohm-cm2 and continued a degradation trend testing back at normal operating conditions.

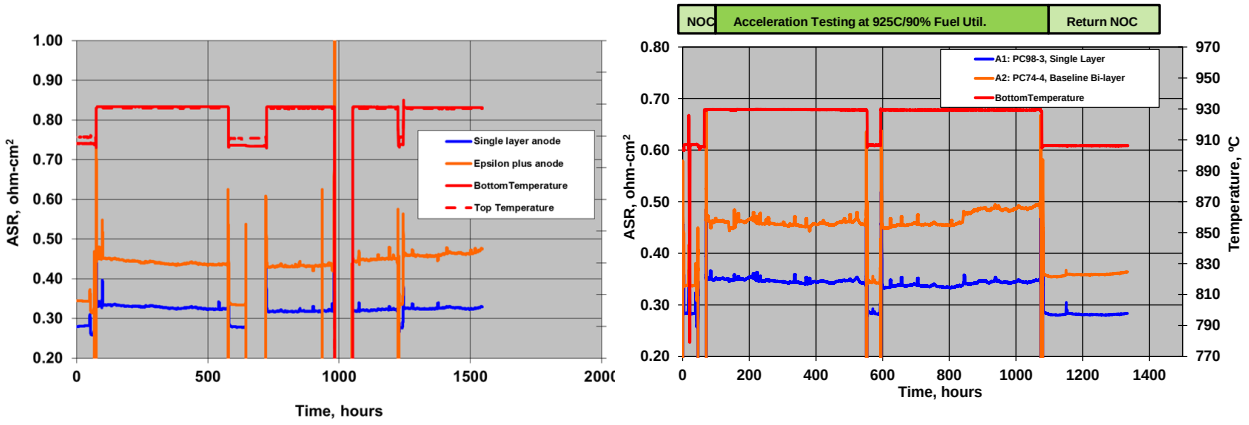

Figure 31. Anode acceleration test, baseline vs single layer anode

As an indicator of anode degradation, detailed microstructure analysis was conducted by CWRU using the cell samples from the acceleration tests. Material distribution across the anode thickness of epsilon bi-layer anode and single layer anode was generated based on 3D reconstruction. Compared to the epsilon bi-layer anode which shows decreased metal content from electrolyte to ACC interface, single layer anode shows more uniform distribution of metal phase across the anode thickness, which may be a factor in the lower degradation rate under aggressive test conditions. From 3D database, anode triple phase boundary (TPB) density was calculated (Figure 32). The anode TPB density after accelerated testing was reduced to ~1.5 m/m^3 from ~4.0 m/m^3 for the as-reduced anode, which is similar to the anode after 5,000 hours of testing under normal testing conditions.

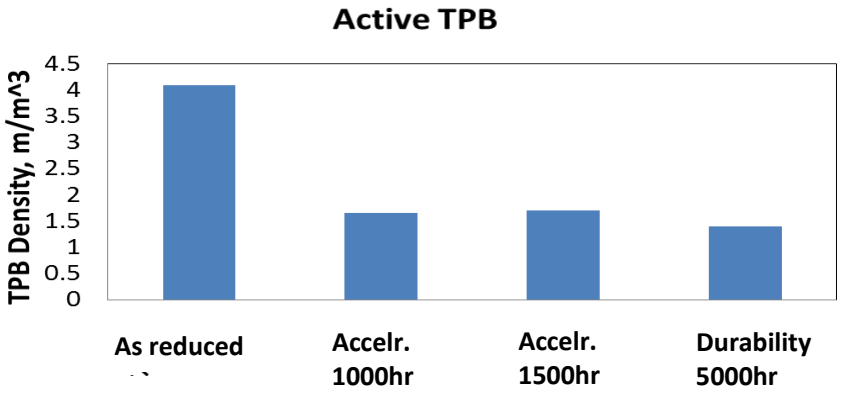

Figure 32. Triple phase boundary length from 3D reconstruction (single layer anodes)

A second methodology for accelerated testing was explored, partly driven by challenges in running the tests at 90% and higher fuel utilizations. Current density was added as a factor while fuel utilization was fixed at a still aggressive 85%. Figure 33 summarizes the ASR change rate after 1,000 hours of duration under testing at normal current density of 380 mA/cm^2 ("NC") versus at a high current density of 530 mA/cm^2 ("HC"). The median value trend shows that the combination of higher fuel utilization and current density resulted in higher ASR degradation rate.

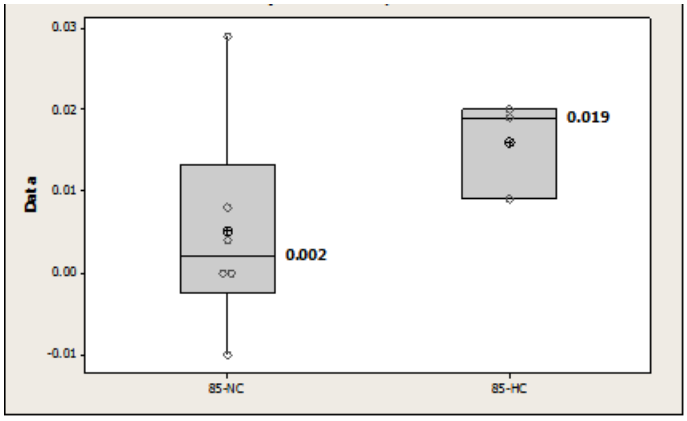

Figure 33. ASR change for 1000hrs for each test matrix in Table 1.

Conclusions – The major outcome of the anode development activities are: (1) low ASR and degradation rate (≤0.2% power degradation per 1000 hours) were demonstrated from multiple pentacells (5-cells in series) with single layer anode through ~17,000 hours of durability test under aggressive system conditions. 2) More detail acceleration test protocol was developed and confirmed that single layer anode can provide more stable performance than epsilon anode and 3) redox tolerance of single layer anode was successfully improved through multiple technical approaches.

Task 3.4 - Cathode Development

Experimental Methods - LGFCS has investigated the degradation mechanism of LSM-based cathodes and examined the influence of A-site dopants, B-site dopants and A-to-B site stoichiometry on the degradation behavior. LGFCS utilized the accelerated testing methodology developed in early stage of the program for screening cathodes for resistance to densification. Case Western Reserve University utilized their state-of- the-art analytical electron microscopy to elucidate the role of free-MnO and LSM surface chemistry changes in the degradation. An expanded understanding of the degradation mechanisms of the various LSM-based cathodes tested for extended periods (>5000 hours) guided selection of a preferred LSM- based cathode to carry forward to entry-into-service (EIS) technology. LGFCS further investigated appropriate classes of mixed electronic and ionic conducting cathodes, nickelates and composites, as a means for achieving a more significant step-change in ASR and/or stack operating temperature. The primary emphasis on nickelate cathodes is the phase stability and electrochemical durability of Ruddlesden-Popper nickelates with the objective being to provide validation of that class of materials as suitable cathodes for commercial SOFC.

Results and Discussion

LSM-based cathode degradation mechanism: Target ASR degradation rates for early product is <8 mohm-cm^2/khrs, but preferably reaching 5 mohm-cm^2/khrs for stack life approaching 5 years. Testing of the baseline (epsilon) cell materials set indicates a rate of 10-15 mohm-cm^2/khrs at conditions of 800-925C, with much of the test data originating under SECA project DE-FE0000303 and continued under this project. Degradation is dominated by cathode changes at block inlet (800C) and mid-point (860C) temperatures, with anode changes contributing significantly as well at block exit (900-925C).

This cathode task has investigated alternate LSM-based cathode compositions for affecting the performance and durability. The primary focus has been the following cathodes with EIS1 and EIS2 receiving the most attention. The LSM cathode current collector is a matched to the LSM phase chemistry of the cathode.

- Epsilon: baseline LSM composition and ionic phase
- Epsilon-plus: change of ionic phase
- EIS1, EIS2, EIS3: LSM composition variants all with the same change in ionic phase as epsilon-plus

In testing between 8000 and 16000 hours and at various scales (penta-cells to bundles) minor differences have been documented in the ASR degradation rates, see Figure 34 for a comparison of representative tests of epsilon and EIS1 and EIS2 cathodes. Post-test analysis and accelerated testing methods have revealed greater differentiation between the cathodes.

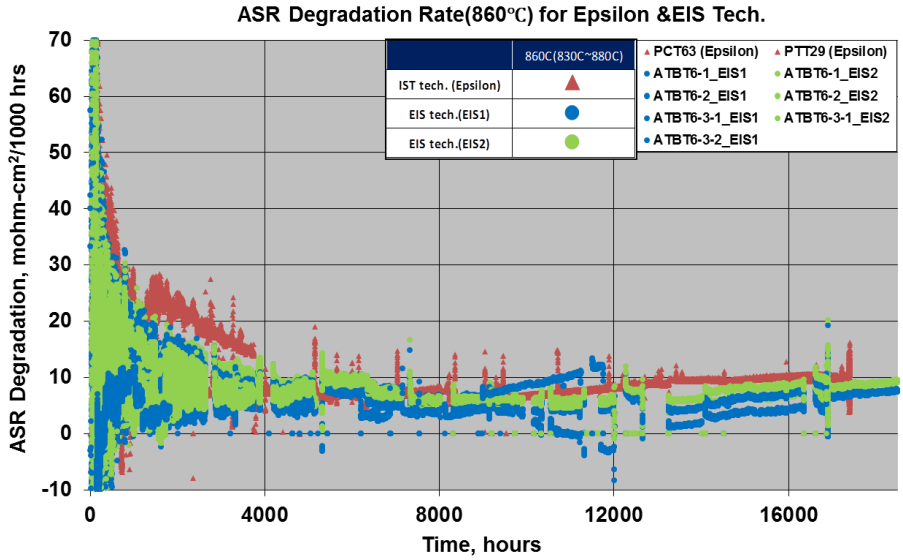

Figure 34. Comparison of 16khr durability of epsilon and candidate cathodes

A detailed post-test analysis of cathodes after two-year long term durability testing was performed both in-house and at Case Western Reserve University (CWRU). Trends observed for the key degradation mechanism are summarized in the following sections:

Mechanism 1: Free MnO_x accumulation near electrolyte interface. Cathode chemistry was analyzed by EDS for the cells tested at different temperatures and duration times focusing on Mn migration. Figure 35 highlights the mechanism where epsilon cathode pentacells were tested at 925C, 4 bar for 5000 hours, one cell held at OCV. Free MnO_x was present throughout the bulk cathode for the cell held at OCV whereas the operated cell showed MnO_x accumulation at the electrolyte interface and loss of free MnO_x from the bulk. The mechanism and driving force for the MnO_x transport/migration is not understood.

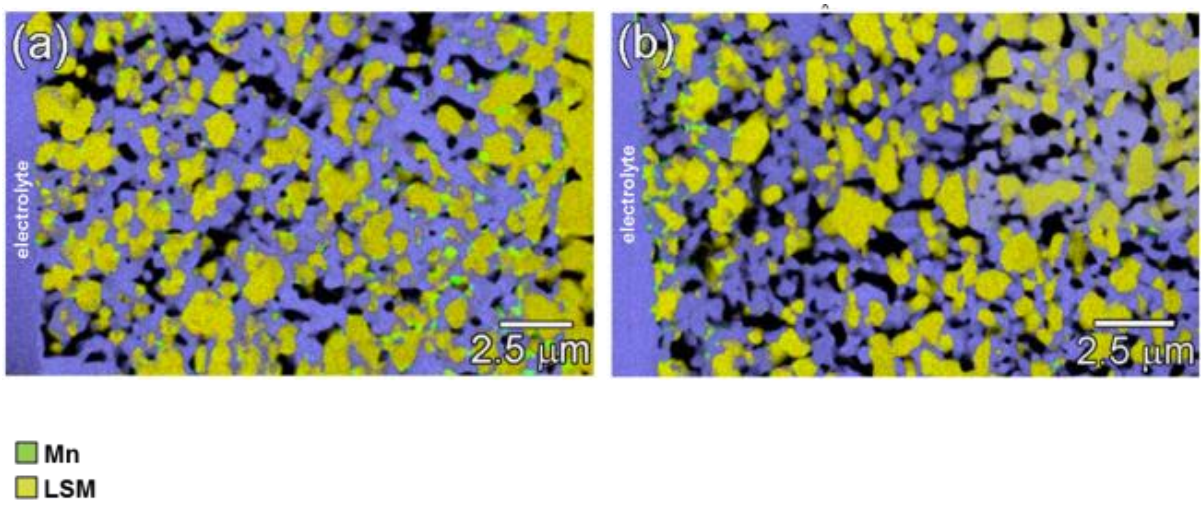

Figure 35. Comparison of MnO_x distribution for epsilon cells at (a) OCV and (b)tested

Figure 36 shows the accumulation of MnO_x at the interface for a tested epsilon cathode cell over time and versus temperature. Quantification of the EDS was performed by large area scans of the bulk cathode and area scans 1 micron deep into the cathode along the electrolyte interface. Figure 37 compares the Mn/La

ratio in bulk cathode and near electrolyte interface vs. duration time for cells tested at different temperatures. The Mn/La ratios are for comparison purposes only, standards were not utilized for accurate quantification, and hence the reason some ratios of Mn/La are less than 1. The Mn/La ratio is generally constant in the bulk cathode during fuel cell operation from start to up to 16,000 hours in the temperature range of the fuel cell block (800-900^{o}C), only a slight change is observed for the epsilon cathode at 900C. At the cathode/electrolyte interface, the Mn/La ratio increases with operating time of the fuel cell for the majority of the LSM-based cathode compositions, with the exception of the EIS2 cathode.

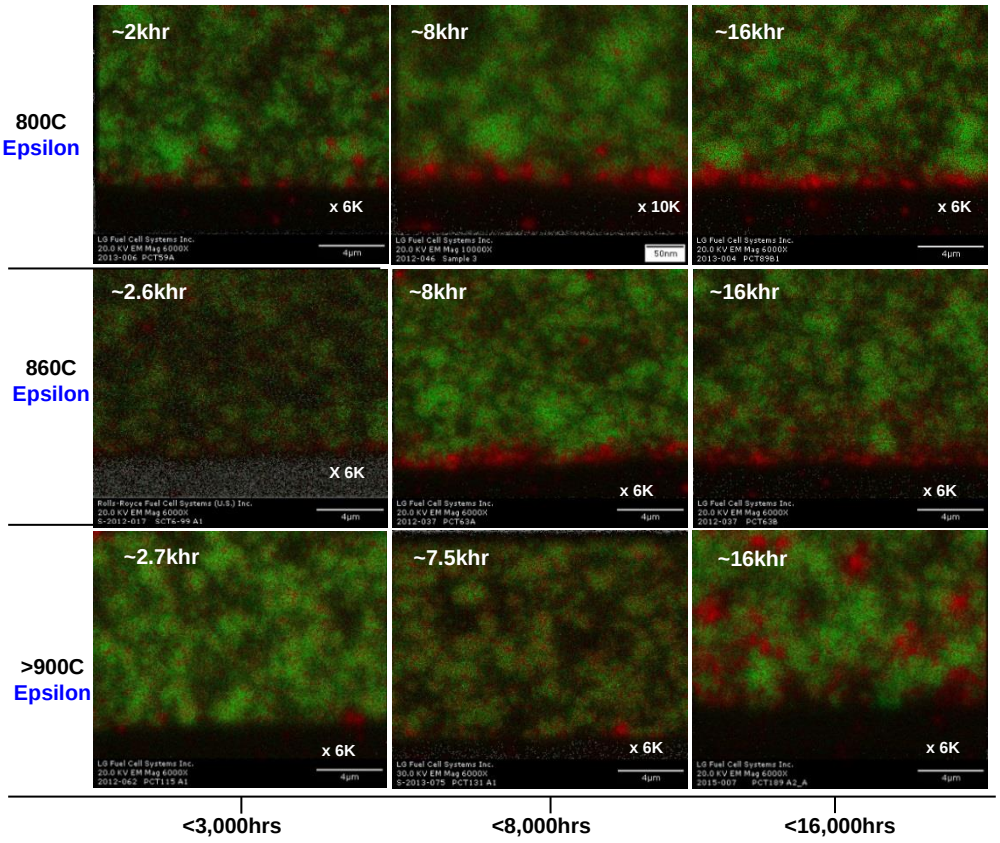

Figure 36. Comparison of MnO_x distribution for epsilon cells with test temperature and time

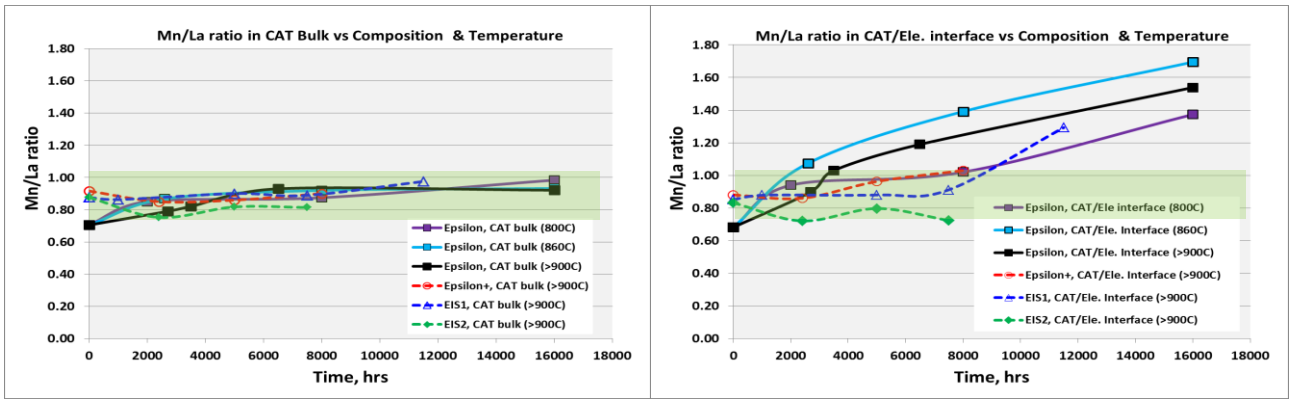

(a) Bulk area of LSM based cathodes (b) Near electrolyte/cathode interface

Figure 37. Mn/La ratio for bulk area of cathodes (a) and near electrolyte/cathode interface (b).

Detailed analysis by TEM provides further comparisons between the various cathodes. Figure 38 shows that the free MnO_x accumulation at electrolyte interface decreased from epsilon cathode to EIS1 and EIS2 cathode.

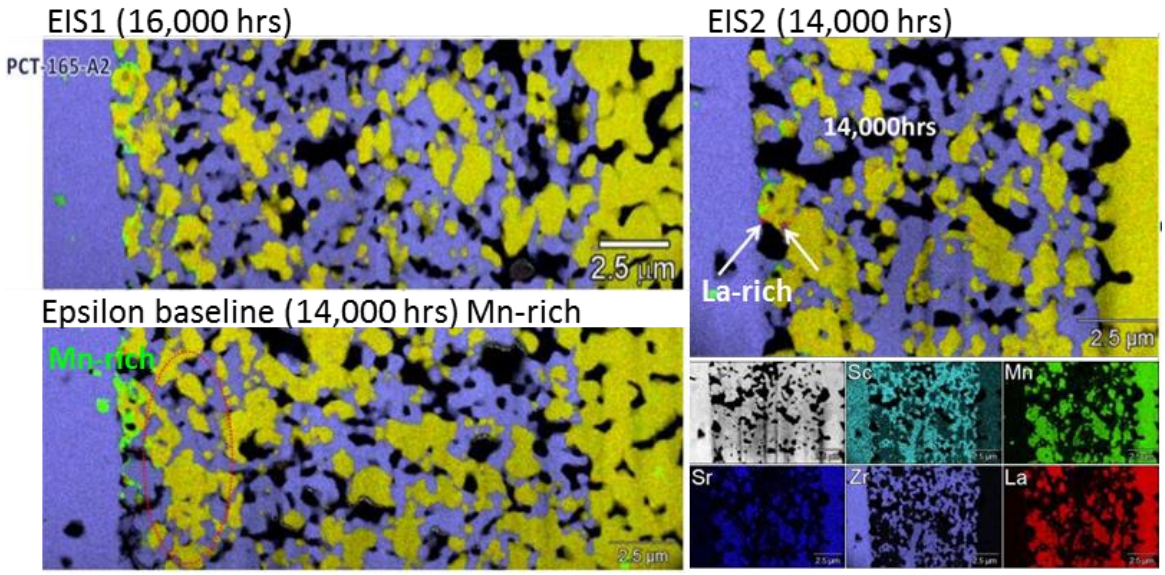

Figure 38. Cathode post-test analysis after long-term durability test at 800°C, 4.0 bara

The composition of the LSM grains throughout the cathode is generally uniform (Figure 39), only a slight reduction in the amount of strontium, especially near the electrolyte interface as measured for an epsilon cathode having been tested 16000 hours at 800C. The free MnOx is not an exsolute from the localized LSM phases.

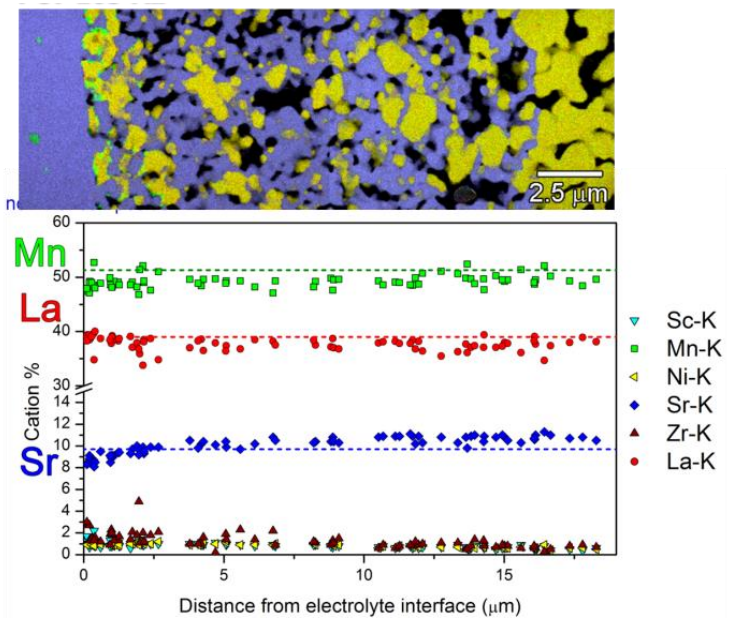

Figure 39. Analysis of LSM phase composition within the bulk cathode

Mechanism 2: Undesired phase formation. The undesired phase formation includes both second phase formation and ionic phase transformation. TEM/EDS analysis revealed phase formation near the electrolyte interface particularly for operation at higher temperatures ≥860°C. Table 4 is a summary of undesired phase formation for LSM based cathodes with operation time and temperature. Undesired phases include La, Zr-rich phase, cation-rich MnO_x and Mn/Cation-rich zirconia. At 800°C only the previously reported free MnO_x phases were observed in testing to 16k hours.

Table 4. A summary of phase formation in LSM based cathodes with time and temperature

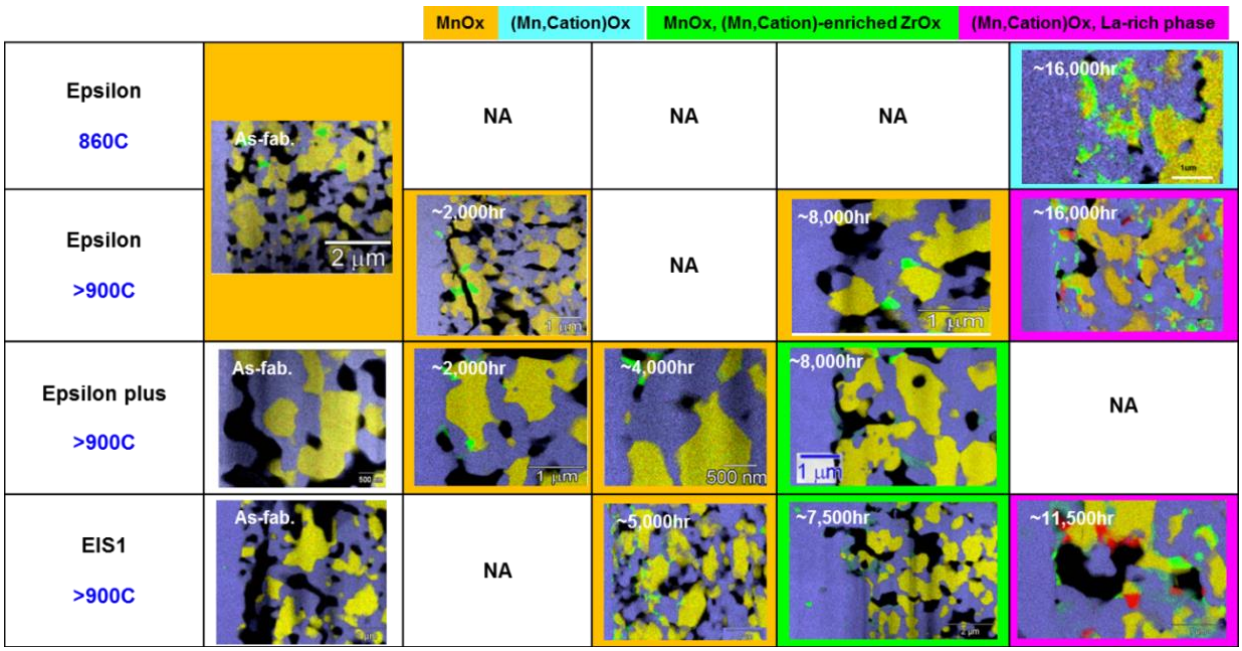

Table 5 is a summary of ionic phase transformation observed with operation time and temperature. Localized transformation of ZrO_2 to monoclinic phase is observed for 900C operation, no detention of monoclinic phases up to 16k hours for cell operation at 800C and 860C, regardless LSM composition. The EIS2 cathode has shown the most resistance to ionic phase changes in testing and analysis to 7500 hours . The results provide further evidence of the benefit of lowering the peak block temperature through a lower block ΔT and shifting to a lower average temperature as facilitated by lower ASR technology.

Table 5. Observed ionic phase transformation of LSM cathodes with time and temperature

Epsilon

Temp.\ Time	As-fab	~2,000hrs	~3,500hrs	~8,000hrs	~16,000hrs
800C	No	Undetectable		Undetectable	Undetectable
860C		NA		NA	Undetectable
>900C		Undetectable	Yes	NA	Yes

Epsilon plus

Temp.\ Time	As-fab	~2,000hrs	~4,000hrs	~8,000hrs	~14,000hrs
800C	No		Undetectable		Undetectable
>900C		Undetectable	Yes	Yes	

EIS1

Temp.\ Time	As-fab	~5,000hrs	~7,500hrs	~11,500hrs	~16,000hrs
800C	No	NA	Undetectable		Undetectable
>900C		Undetectable	Yes	Yes	

EIS2

Temp.\ Time	As-fab	~5,000hrs	~7,500hrs	~14,000hrs
800C	No			Undetectable
>900C		NA	Undetectable	

Mechanism 3: Cathode densification near electrolyte: Post-test analysis indicates that cathode densification occurs near the electrolyte/cathode interface under certain operating conditions. Densification is most pronounced for test times exceeding 7000 hours and at temperatures >860C. No cathode densification was observed at 800°C up to 16,000hrs operation regardless LSM composition. With longer operation time, the densified layer thickness increases. Both free MnO_x formation and cathode densification may be related to LSM phase instability under lower pO_2 and continued sintering.

An accelerated testing methodology has been developed at LGFCS for materials screening to improve cathode long term stability and avoid cathode densification near the electrolyte interface. Parameters varied are current density, temperature and cathode environment, including Cr contaminants in some cases. Initial cathode screening was performed using symmetric button cells. In one test rig, three symmetric button cells are installed in series. Four accelerated tests are summarized in Figure 40. The total ASR change for three cells connected in-series can provide some indication of combination of cells having improved durability under the accelerated conditions. The cell combinations that contain the epsilon cathode show high degradation in shorter duration than in tests with EIS candidate cathodes. Post-test analysis used to compare degree of the cathode densification mechanism and the epsilon cathodes have consistently shown an enhanced tendency towards densification. From such testing, it was determined that the EIS3 exhibits resistance to densification.

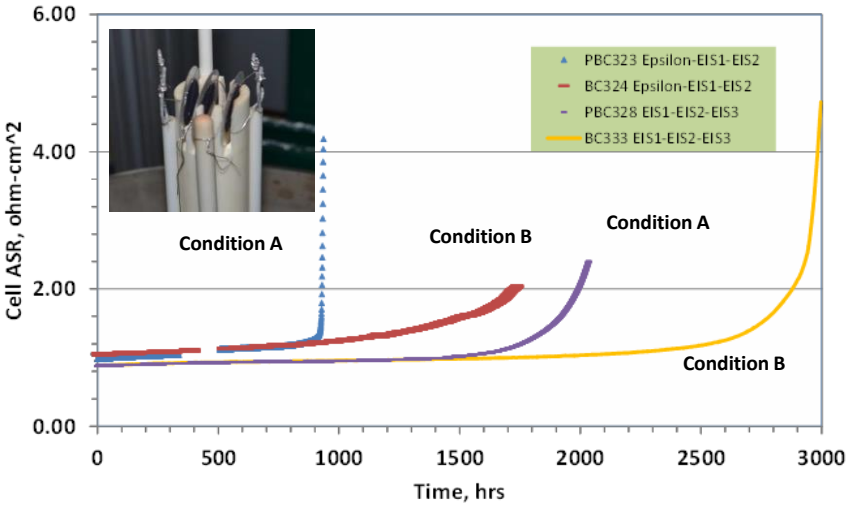

Figure 40. Summary of accelerated test under new testing condition

Following the acceleration testing results, the various cathode compositions were tested side-by-side in subscale testing, while maintaining accelerated testing conditions of 925C, 760 mA/cm^2 and under air (1bar) . In two tests (Figure 41) the EIS3 cathode has shown a lower degradation rate than other candidate cathodes and post-test analysis confirms a more stable cathode microstructure than the baseline.

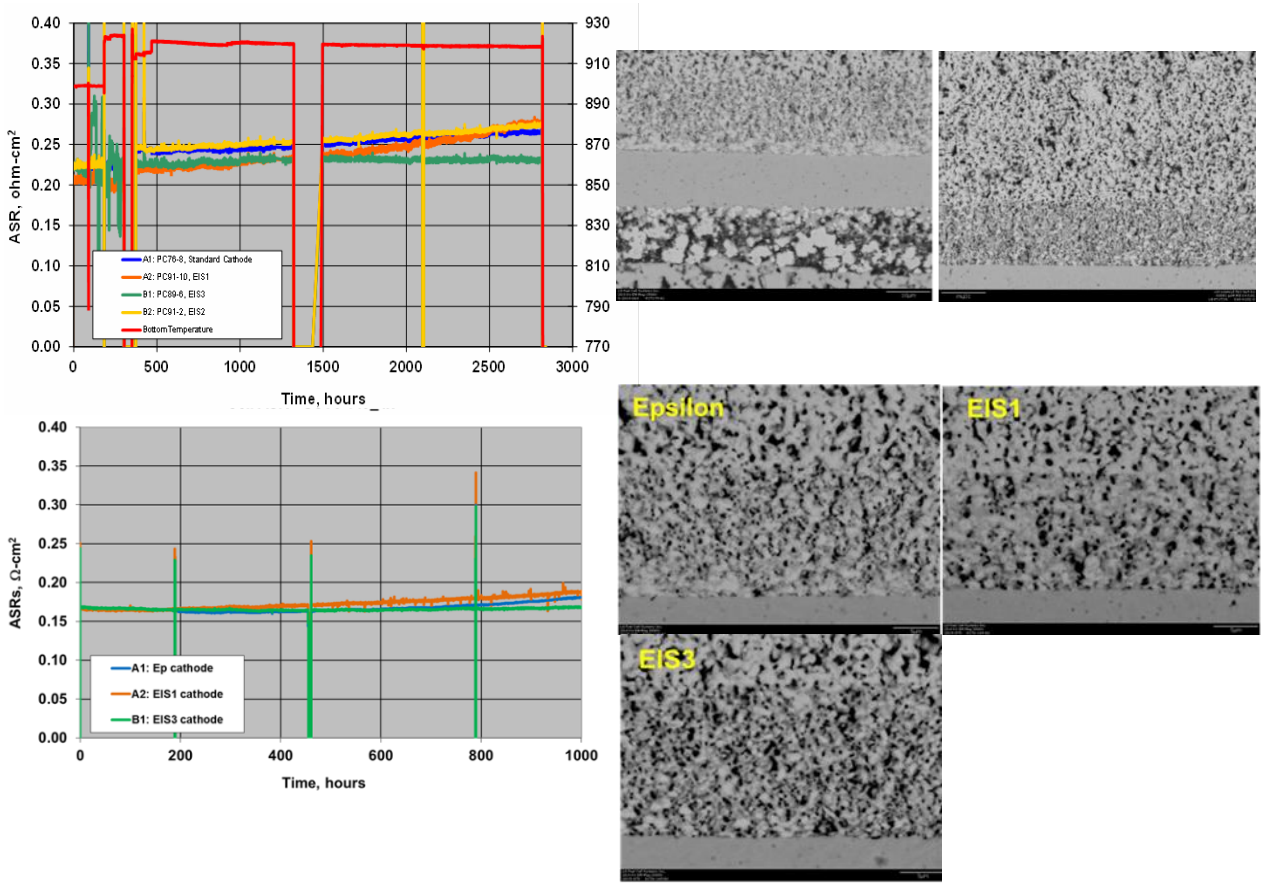

Figure 41. LSM based cathode subscale accelerated test

Verification of degradation mechanisms: The effect of cathode densification on degradation or cathode polarization was confirmed through designed experiments. A series of symmetrical cells having normal cathode layer with expected porosity (CA) plus dense cathode layer near electrolyte (DL) were made and cathode polarization was measured. The objective is to intentionally introduce a dense layer between cathode and electrolyte using the same material as the epsilon cathode to simulate the cathode densification obtained during long term operation and to better understanding its effect on degradation. Both 8 and 15 micron thick epsilon cathodes were used as baseline cases for non-densified cathodes. The dense cathode layer generated was from 3.5 to 7 microns thick. The e-chem results of these symmetrical cells with different thickness of dense layer and combination with layer thickness of normal cathode were summarized in Figure 42. The cathode polarization increased with increasing dense cathode layer, for both 15 and 8 micron thick cathodes.

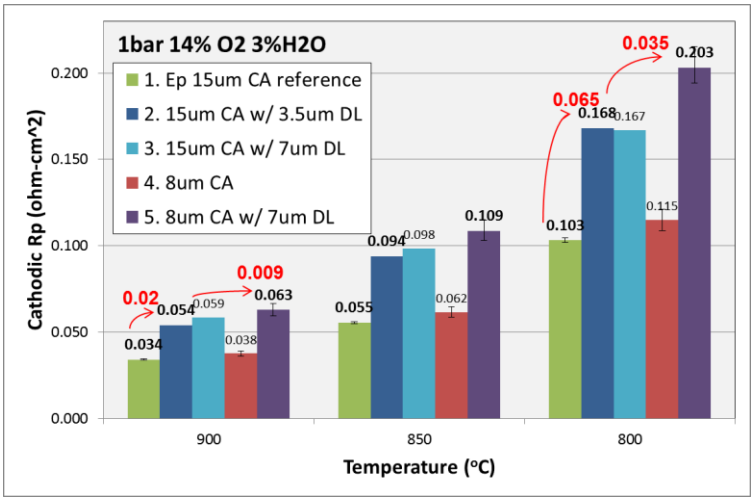

Figure 42. Rp of epsilon cathode with dense layer (@ 1bar 3%H2O 14%O2 ratio)

The effect of free Manganese oxide formation near electrolyte interface on cell performance was also investigated. Symmetric button cells were fabricated by mixing epsilon cathode with 10 wt.% MnO_2, and the e-chem test results are shown in Figure 43. Cathode polarization resistance change induced by adding MnO_2 in Epsilon cathode is insignificant at 900°C and increases ~15% at 800°C. These levels of Rp change are not representative of the cell ASR changes observed in the long-term durability tests. The correlation between free MnO_x formation/accumulation along with cathode densification needs further investigation, and there could be a combined mechanistic effect.

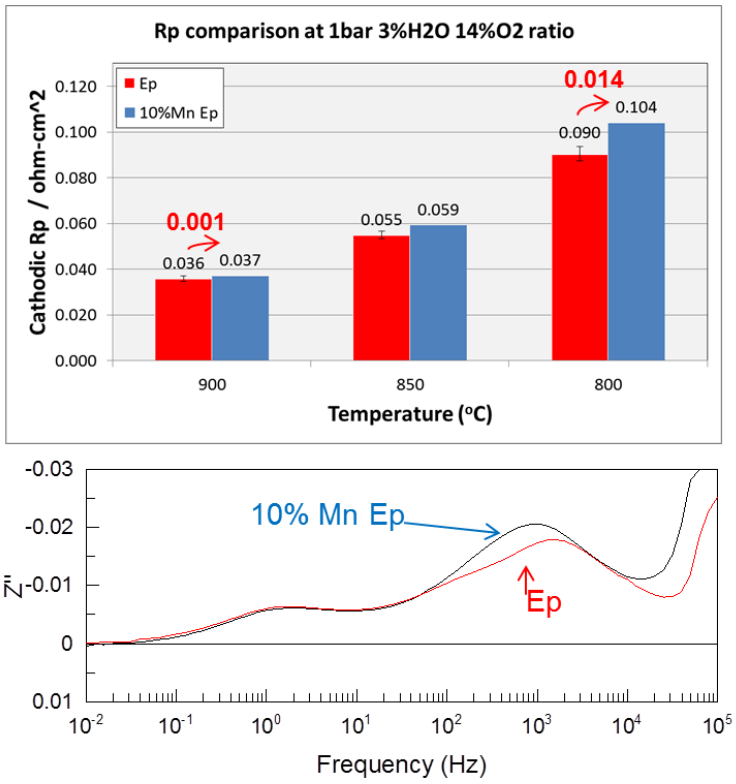

Figure 43. Button cell performance of epsilon cathode mixed with 10 wt.% MnO_2

Cr effect on cathode degradation: In LGFCS's cell design, there is no metallic interconnect, however the Cr species generated from balance of plant can affect LSM-based cathode performance. To understand the effect of Cr on cathode degradation, test rigs were modified to include a Cr source for testing of subscale cells (5-cell in series) to mimic system conditions. Figure 44 summarizes a durability test performed at 900C, 4 bar including epsilon, epsilon plus, EIS1 and EIS2 cathodes. WDS analysis was performed after the 2100 hour test. The lowest degradation was observed for the EIS2 cathode and it exhibited the lowest Cr contaminant levels at the cathode-electrolyte interface. The EIS2 cathode has the least tendency for free MnO_x formation and this may be a factor in its lower Cr pick-up.

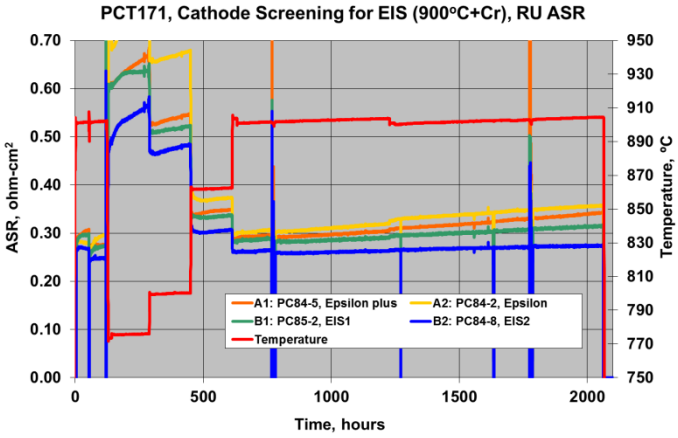

Cell ID	PCT171A1	PCT171A2	PCT171B1	PCT171B2
Cathode	Epsilon plus	Epsilon	EIS1	EIS2
CCC	ε	ε	ε	ε
Surface CCC	1.514	0.859	0.572	0.423
Bulk CCC	1.431	0.734	0.636	0.438
CCC/cathode	1.200	0.722	0.496	0.322
Bulk cathode	1.873	0.660	0.458	0.269
Cathode/electrolyte	2.655	0.888	0.799	0.428
Electrolyte	0.032	0.034	0.034	0.040

Figure 44. Cr-contaminant test at 900C, 4bar and post-test WDS Cr deposition analysis

The goal is to gain an understanding of acceptable Cr contaminant levels within the cathode that will still allow meeting service life requirements. Such information can then guide how effective chromium mitigation strategies for the balance of plant components and chromium getting need to be. From subscale (5-cell) testing in chromium containing environments, a database is being generated for ASR degradation rates as a function of chromium levels detected within the cathode and near the electrolyte interface (Figure 45). The degradation rate target for commercial products is <5mohm-cm^2/khrs. As the baseline degradation of the LSM cathodes is in the 10mohm-cm^2/khrs range, the plot would then suggest that Cr-contamination levels within the cathode should be kept to very low levels, likely under 0.25 atomic percent

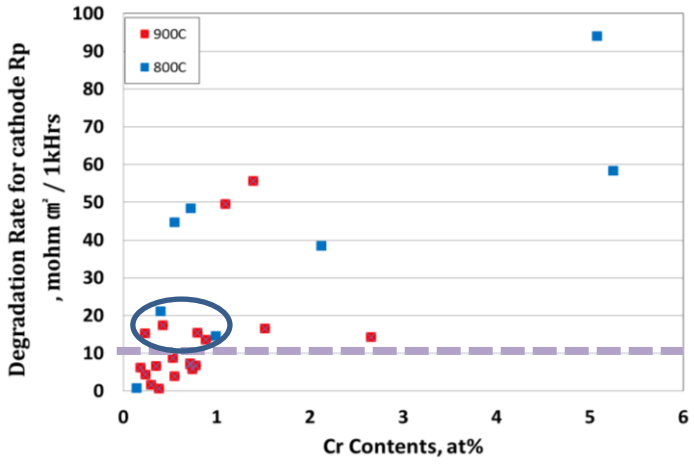

Figure 45. ASR degradation rate for Cr exposure tests, measured Cr contamination levels

Nickelate cathodes: Lanthanide nickelates having the general formula $Ln_2NiO_{4+\delta}$ may have a layered structure with alternating layers of perovskites and sodium chloride type layers. The interstitial oxide-provide for highly mobile O^{2-} an exhibits good ionic conductivity. Moreover, in this structure, the Ni (III)/Ni (II) redox couples are pinned at the top of the O^{2-}: 2p6 bands to give an acceptably high electronic conductivity in the mixed-valence state. Due to its unique structure, lanthanide nickelate cathodes may have lower activation energy than other cathode materials being used for solid oxide fuel cells, such as LSM and LSCF. Especially low ASR has been demonstrated from praseodymium nickelate cathode which may be less dependent on temperature change than other materials. However, one issue is that nickelate materials can be unstable under fuel cell operating temperatures, such as between about 700 to about 900 degrees Celsius. Further, under fuel cell operating conditions, the favorable phase of the nickelate cathode tends to decompose into undesired phases, which causes fuel cell performance degradation.

Pr_2NiO_4 nickelate has lower ASR than other nickelate compositions, such as Nd_2NiO_4 and La_2NiO_4, which is especially attractive to fuel cell developers. However, its phase instability is a hurdle for commercialization. The schematic (Figure 46) shows Pr_2NiO_4 phase decomposition and the formation of PrO_x and NiO during fuel cell operation and actual post-test analysis of a Pr_2NiO_4 cell with significant degradation at 775C.

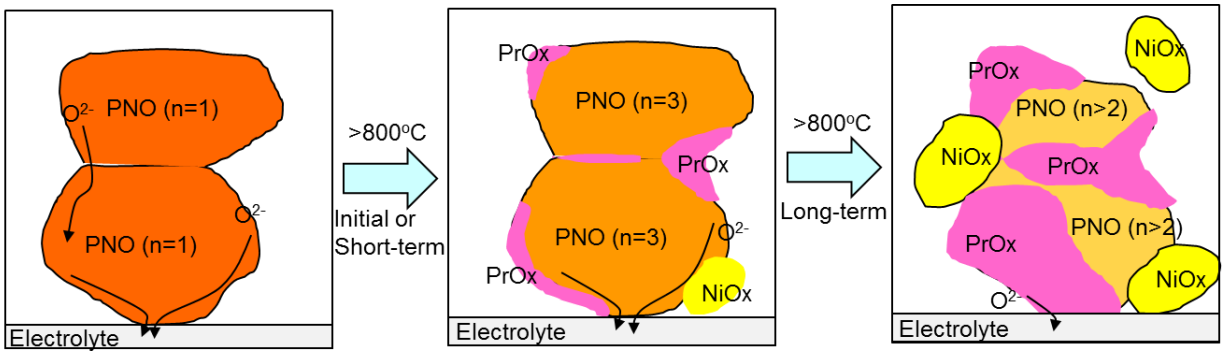

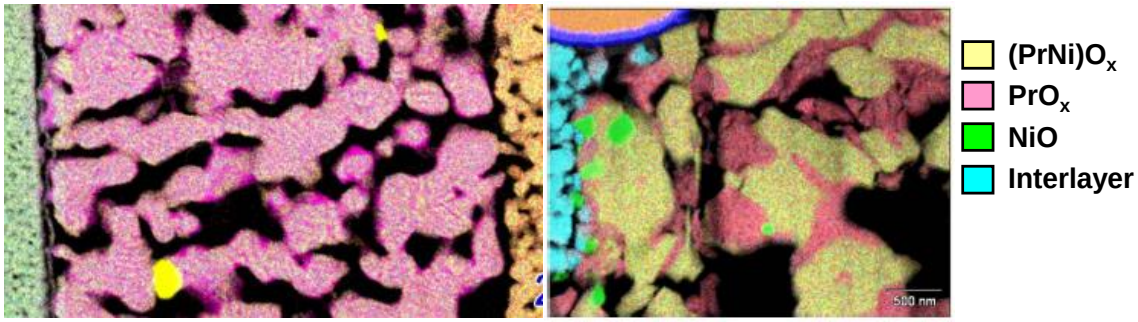

(a) 790°C for 120 hrs (BC271) (b) 775-900°C for 1,500 hrs

Figure 46. Scheme of decomposition phenomena of nickelate cathode, Pr_2NiO_4

To improve nickelate cathode long term durability, LGFCS has identified the following technical approaches to improve nickelate cathode microstructure, manage phase composition, and reduce degradation rate.

1) A or B site doping to improve phase stability
2) Form composite cathode.
3) Manage chemical interactions, interdiffusion between the ceria and nickelate compounds
4) Optimization of interlayer to manage material migration and phase composition

LGFCS investigated various nickelate cathode chemistries, or composites, in an effort to narrow in on a composition that achieves good phase stability and also exhibiting a favorable microstructure and interface connection to the barrier layer. Nickelate cathode materials prepared by above approaches has been classified by TEM and XRD analysis as an initial phase stability test. These technical approaches were proved to be effective and significant progress was achieved. More detailed results will be described in following sections.

Nickelate cathode performance mapping: LGFCS performed button cell tests to screen a variety of nickelate cathodes encompassing the technical approaches outline above. From button cell test, cathode polarization (Rp) and short-term durability data were generated. Based on XRD and TEM analysis (by CWRU) of aged nickelate pellets, second ionic phase, type I and type II, were selected to form composite – I and composite – II cathode with nickelate, respectively. Figure 47 compares Rp of nickelate and its composite cathodes (with second ionic phase type I or II) in symmetric button cell test. Class A nickelate composite cathode with second ionic phase (type I, or type II) showed Rp of 0.015 ohm-cm^2 at 870^{o}C, which is similar to the ASR value of nickelate A cathode (non-composite). By the addition of second ionic phase, improved long term durability is expected due to an improved interface, a more stable microstructure and retention of desired phase.

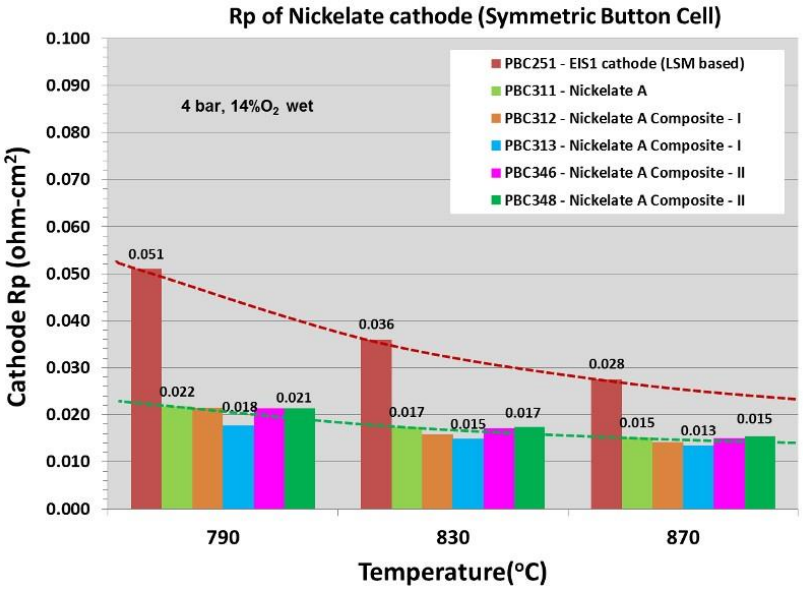

Figure 47. Rp comparisons for class A nickelate and its composite type I & II in button cell test

Different cathode barrier layer materials were investigated to achieve lower ASR and degradation rate. TEM analysis of tested button cells and subscale cells by CWRU identified potentially preferred barrier

layer compositions to be matched to nickelate cathodes. Figure 48 compares the Rp of Nickelate A and B cathodes (different nickelate formulation) in symmetric button cell test with different barrier layers. Barrier layer B showed a lowering of cathode polarization (applied to Nickelate B) due to improved interface and material migration. A short-term durability test using nickelate B cathode on barrier layer B showed lower degradation rate of 7.0 mohm-cm^2/1000hr at 790 ^{o}C for 150~200hr, compared to the same nickelate cathode on barrier layer A, 36 mohm-cm^2/1000hr.

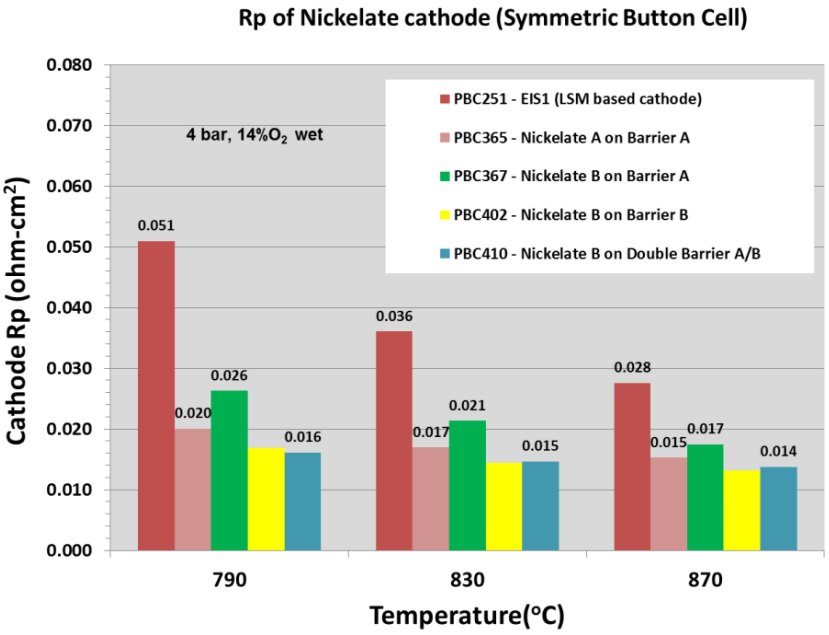

Figure 48. Rp comparisons for class A and B nickelate with different barrier layers (button cells)

From above preliminary database of button cell tests, subscale tests (5-cells in series) of candidate nickelate compositions with LNF as CCC layer were tested to achieve low ASR and degradation target for future technology. Figure 49 is the summary of cell ASR vs temperature generated by subscale cells to compare nickelate cathodes and LSM based cathodes (EIS1). Candidate nickelate cathodes showed lower ASR and activation energy providing the possibility to operate at lower temperature range for longer service life. The average ASR of nickelate cathode at 860^{o}C is 0.192 ohm-cm^2 (±0.019) vs. 0.240 ohm-cm^2 for LSM-based cathode at 1bara and ambient air with 3% H_2O. Nickelate A composite cathodes with a second phase (type I or II) are most promising for low ASR. Lower cell ASR with nickelate cathode was also achieved when tested under system conditions of 4 Bara, see Figure 50. In this test, subscale cells with nickelate cathode and LSM-based cathode were installed in the same test rig and tested side-by-side (PCT197). Average cell ASR is 0.168 ohm-cm^2 at 860^{o}C for nickelate cathode, meeting the project milestone of a 0.02 ohm-cm^2 lower ASR.

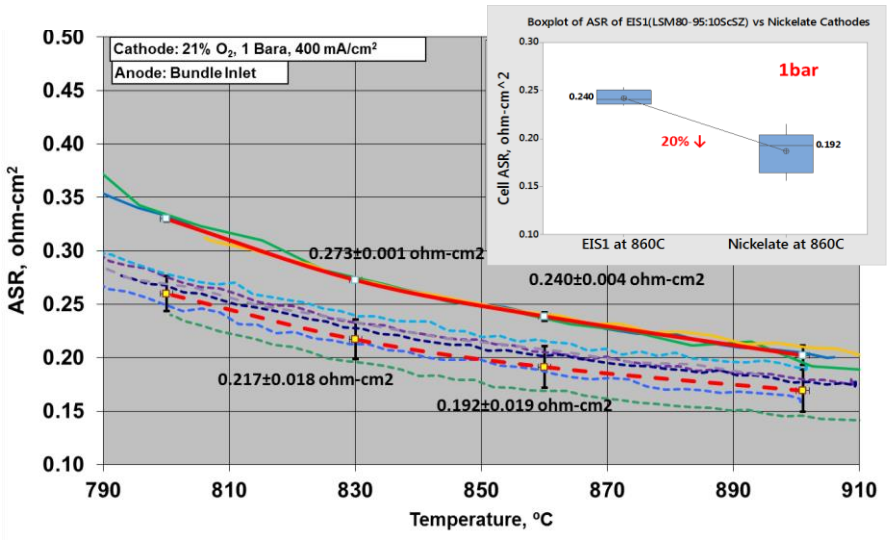

Figure 49. Nickelate and composite vs. LSM cell ASR at 1 bar

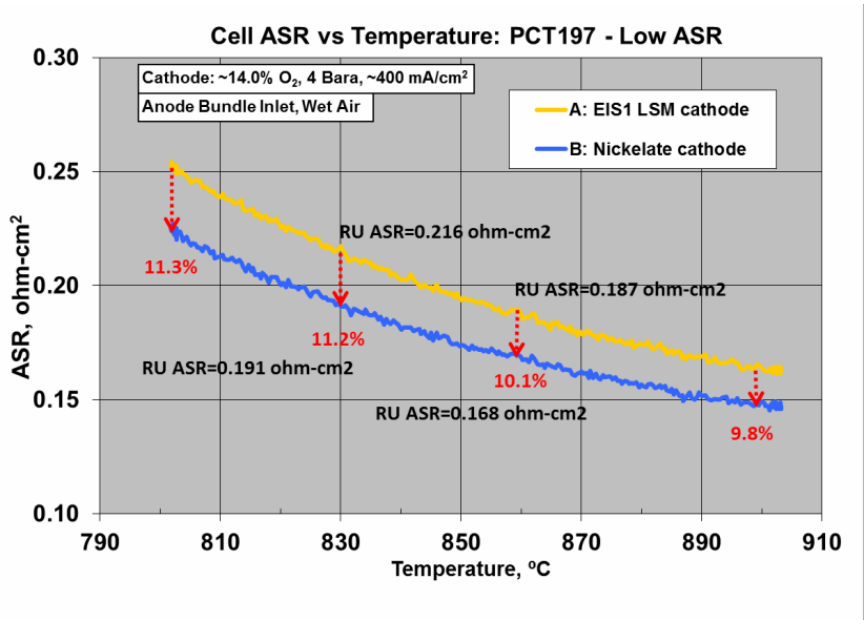

Figure 50. Nickelate composite vs. LSM-based cell ASR at 4 bar

Durability assessment: Durability testing was run on the button cells for ~200 hours to obtain preliminary comparisons before moving to subscale substrate tests. Figure 50 shows the compilation of the cathode polarization, Rp, and button cell degradation data for the various combinations of nickelate cathode compositions, composite cathode combined with different barrier layer composition. Several of the nickelate (composite) compositions show lower degradation rate, see the blue box in Figure 51.

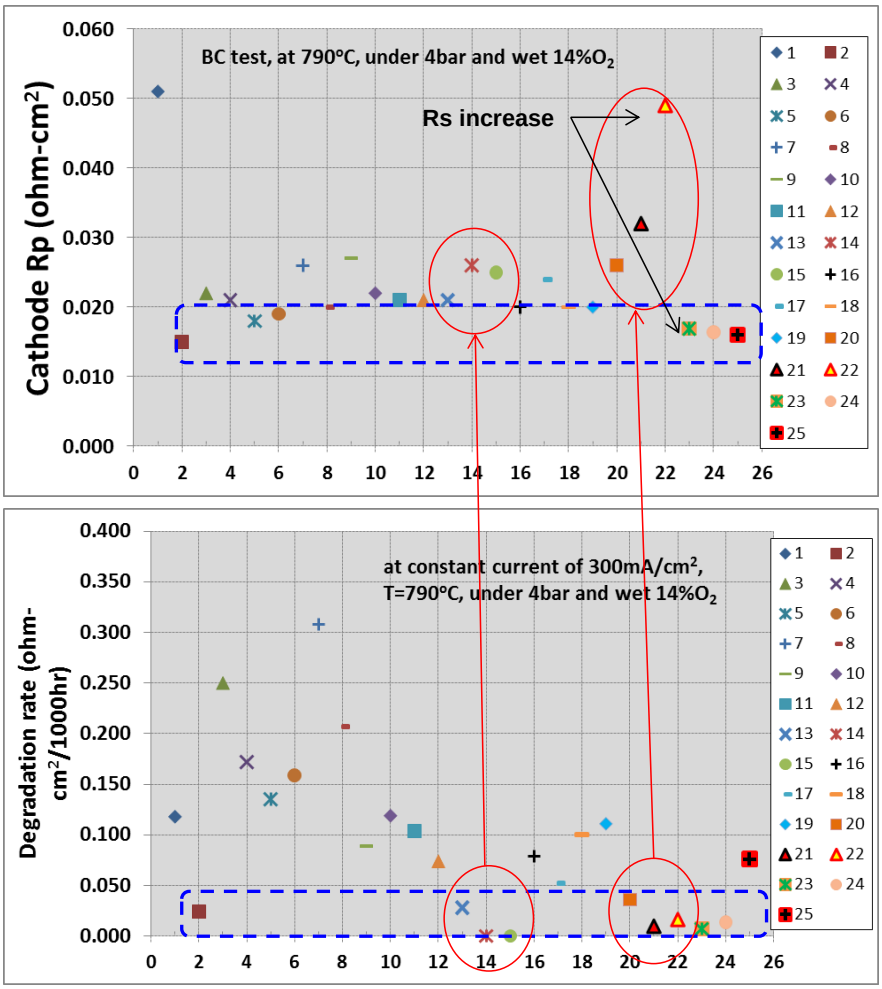

Figure 51. Nickelate Rp and degradation data generated for button-stage screening

Based on the preliminary database of button cell tests, both cathode Rp mapping and the durability, subscale tests (5-cells in series) of candidate nickelate compositions were fabricated using optimized LNF CCC layer. Figure 52 is a durability result for candidate Nickelate A – Composite I cathode operated at 1 bar, bundle mid-point fuel composition, and air with 3%H_2O at 860°C. The degradation rate to 9500 hours was 6.1 mohm-cm^2/1000hr, comparable to LSM-based cathode. Cathode polarization is generally stable during 9,500 hours of operation except for a minor step change at around 2,000 hours due to an air trip event.

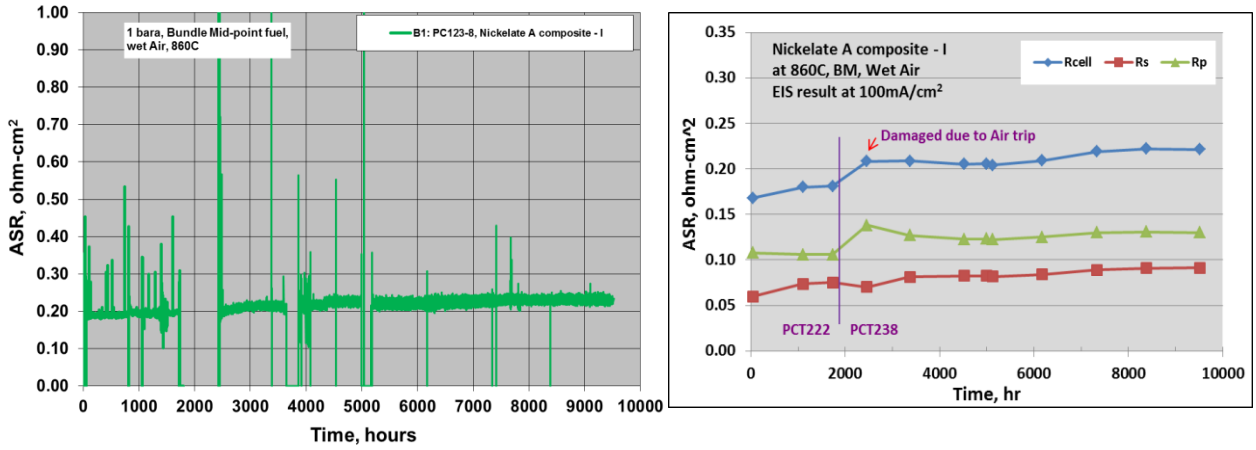

Figure 52. Long-term durability for nickelates and its composite cathodes (860°C, 3% H_2O)

A repeat long term durability test of nickelate A composite I was performed (Figure 53) along with a comparison to nickelate A composite II cathode. A similar degradation rate as the initial test, 6.0 mohm-cm^2/1000hr, was measured for the A1 cell (nickelate A composite I) and 12.7 mohm-cm^2/1000 hr for A2 cell (nickelate A composite II). Post-test analysis of the 9500 hour nickelate A-composite I and 7000 hour nickelate A composite II indicates that the degradation rate difference may be attributed to the microstructural difference (Figure 54). The nickelate A composite-type II cathode shows larger nickelate grain size, less triple phase boundary, and a weak interface between cathode and cathode barrier layer. Whereas the nickelate A composite-type I cathode has a finer and good adhesion to the cathode barrier layer. This test confirmed that it's feasible to improve nickelate cathode long term degradation/durability through phase and microstructural management. A promising ASR degradation rate was obtained even in the presence of phase changes, implying that the altered phase compositions themselves exhibit favorable electrochemical activity. Similarly low degradation rates of 6-8 mohm-cm^2 have been obtained with alternate barrier layers in shorter term tests.

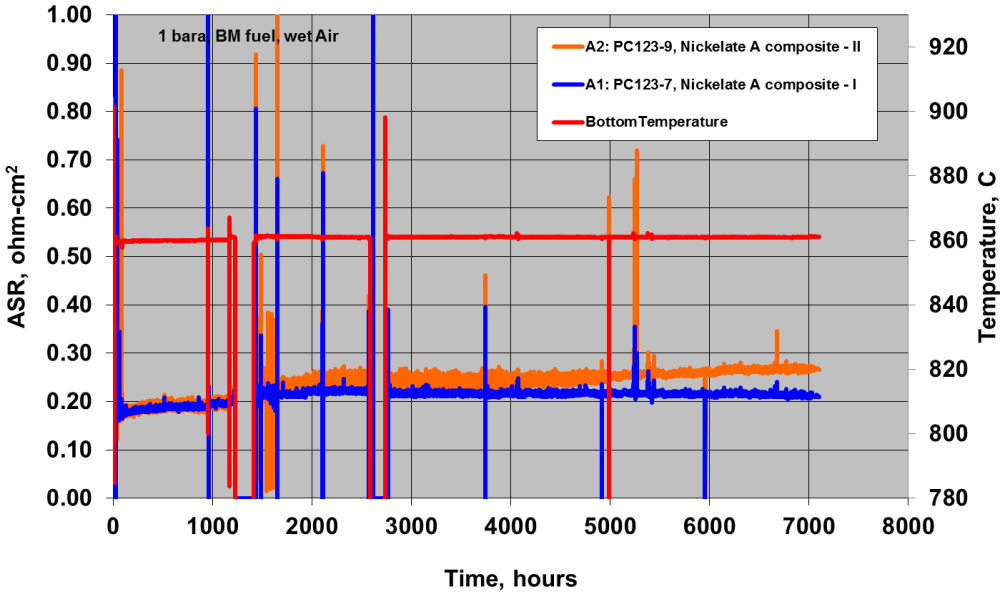

Figure 53. Long-term durability for nickelates and its composite cathodes (860°C, 3% H_2O)

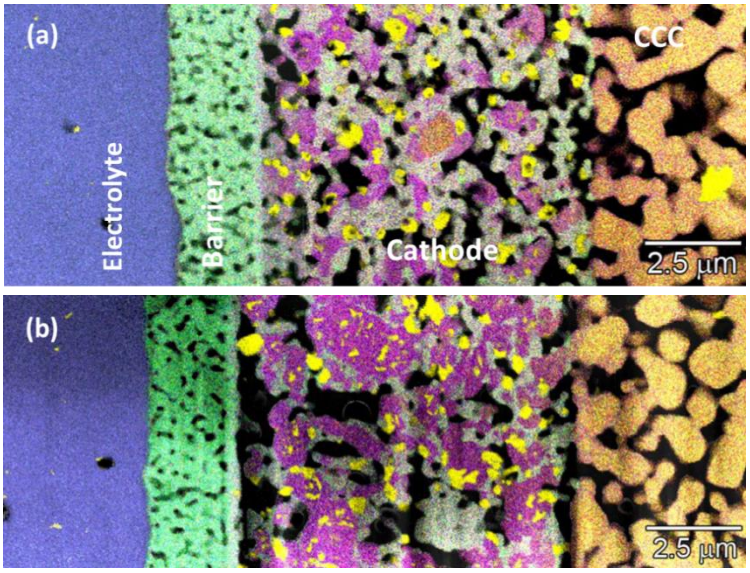

Figure 54. TEM images 860C testing
(a) 9500hr Nickelate A Composite – I (b) 7200hr Nickelate A composite - II

LGFCS has further refined the composition of the nickelate phases and the compositing with the ionic phase to achieve enhanced phase stability. Figure 55 shows a TEM image of the newest nickelate composite cathode following heat treatment for 500 hours at 870C. This composition went into electrochemical testing at the end of the project period.

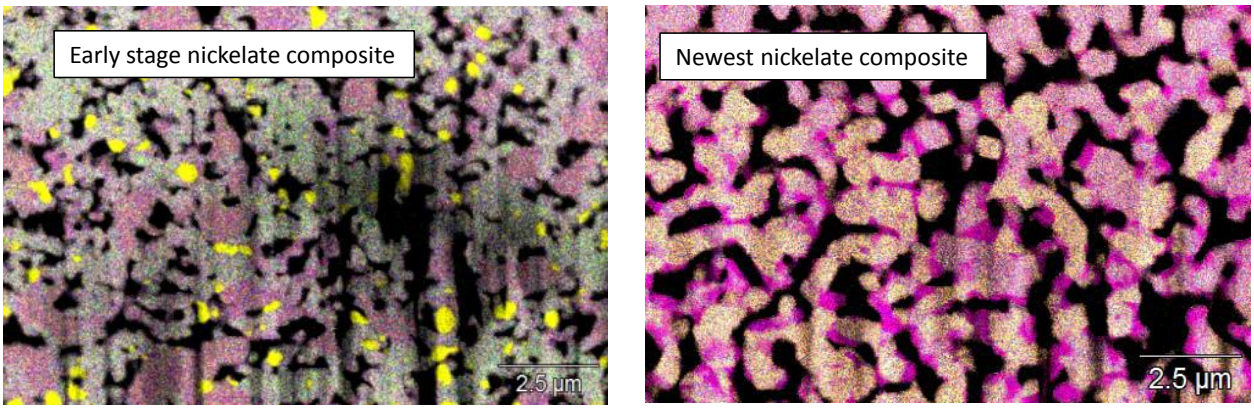

Figure 55. Improved phase stability of newest nickelate composite cathode

Conclusions – Three primary mechanisms (MnO_x migration, cathode densification and localized ionic phase changes) drive cathode degradation. Candidate cathode compositions have been evaluated under normal operating conditions and accelerated testing conditions, showing various degrees of impact from such mechanisms. Electrochemical testing, coupled with the post-test analysis has identified improved cathodes compared to the historic baseline composition. Candidate compositions are now being carried into TRL5 and TRL6 testing having the complete representative environment of product (inclusive of contaminants), and to serve as the next stage of selection/validation of cathodes for product

introduction. More importantly, the studies supported by this project is leading to selection of new round of candidates for TRL3-4 testing to investigate materials for even lower degradation rates, targeting <5 mohm-cm^2/khrs.

Nickelate composite cathodes with various second phases were evaluated for both polarization and durability. A selected nickelate composite cathode shows a 10% lower ASR than the best LSM-based cathode, and it has a comparable degradation rate in the system operating temperature range. TEM analysis indicates significant microstructural stability and lower degradation rate for nickelate composite cathode even though phase changes occur during testing. Addition of second ionic phase and optimization of barrier layer were proved to be effective approaches to manage nickelate phase composition and improve microstructure to achieve longer service life.

Task 4.0 – Block Testing

Experimental Methods – Pressurized block-scale test rigs present in Canton, Ohio and Derby, UK were utilized for performing the metric tests. The block tests will be run on a reformate fuel representative of that for the market entry 1MW natural gas system. Two block tests will be performed during the program:

1. Block metric test – LGFCS will complete a 4-strip block (~15 kW) metric test, carried over from DE- FE0000303, with the objective of achieving 5000 hours of operation. The target degradation rate is ≤1.5% per 1000 hours.

2. LGFCS will perform an additional block test at 15 kW that incorporates the selected active layer material sets and designs for improved durability targeting a power degradation rate of <0.75% per 1000 hours. A minimum test duration of 2000 hours is scheduled.

The block test rig (Figure 56) used for the metric test matches the MW-scale system cycle, and is in fact often termed a mini-tier rig as it matches the basic design features of the 250 kW pressurized tier but contains a single block being the repeat unit within the 250 kW tier. The block rig contains representative ejectors, reformers, heat exchanger, off-gas burner and insulation components and as such constitute a representative environment with respect to contaminants such as chromium and silica. The heat input into the blocks that is provided by the turbo-generator in the full system is replicated by electric heaters for the block test rigs. The block test rigs are thermally self-sustaining when accounting for the system equivalent heat input from the electrical heaters. The block tests rigs used under this project contain an old block design having an air by-pass issue causing less cooling air to the strips. To compensate, the blocks were run with 4 rather than 5 strips to achieve design point temperature distribution.

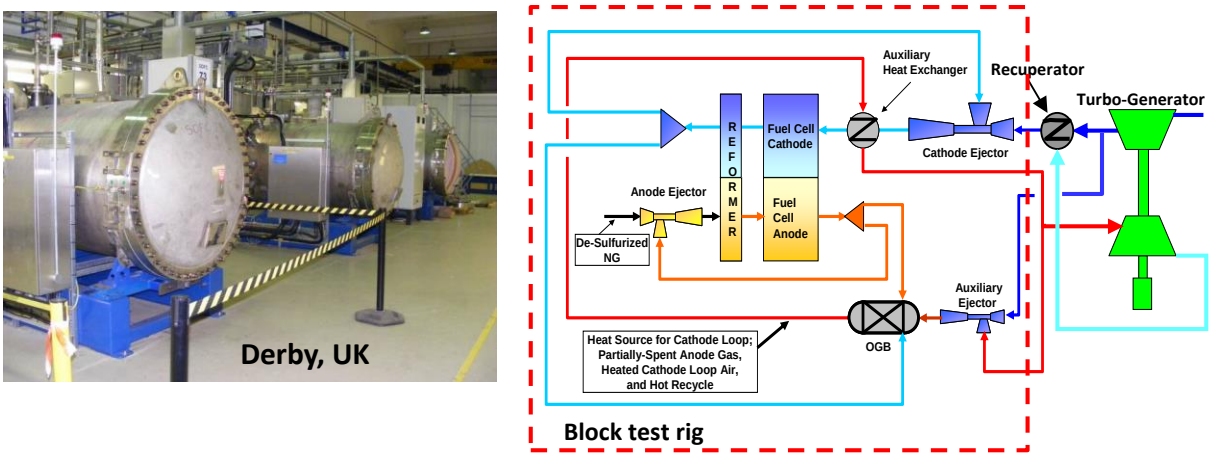

Figure 56. UK block test stand configuration and cycle match to system

Results and Discussion

Canton Test (LGFCS #T1418): This test is classified as the carry-over test. Three of the strips were of the baseline epsilon technology and 1 strip (in position 1, block inlet) has the candidate entry-into-service cathode EIS1, lower ASR primary interconnects and new secondary interconnections for improved reliability. The test reached 1445 hours at which time it was shut down for a non-stack related issue. The power degradation through 1445 hours of testing was 1.32%/1000 hours (Figure 57), under the target of 1.5%/1000 hours. Starting ASR was only 0.27ohm-cm^2 (Figure 58).

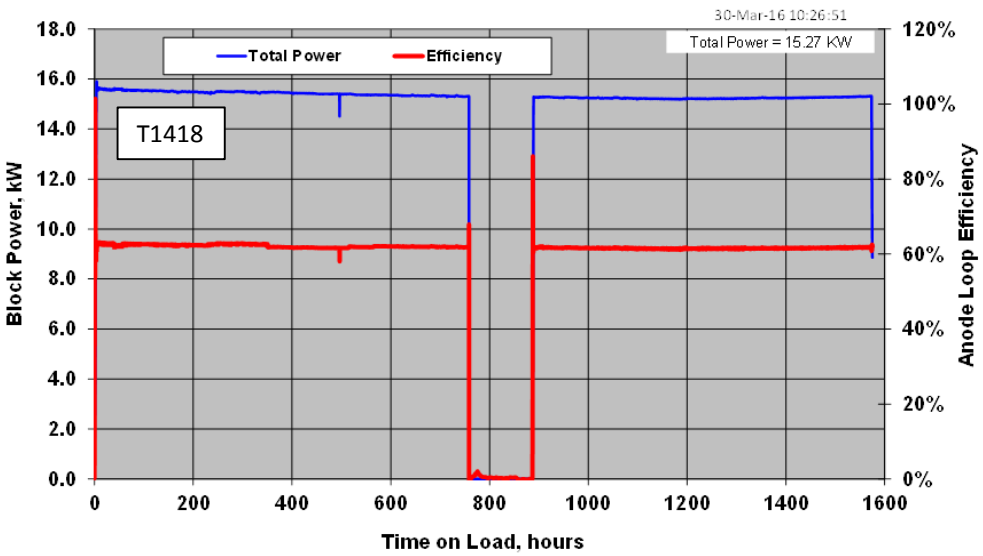

Figure 57. T1418 power and efficiency plot

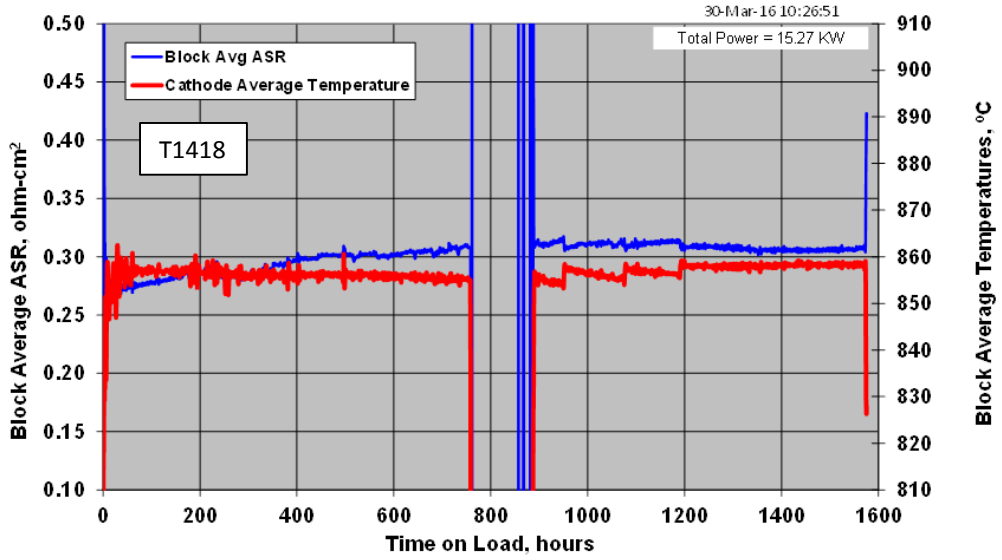

Figure 58. T1418 ASR and cathode temperature plot

UK Test (LGFCS Block T1315): This test is the additional DE-FE0012077 block test incorporating candidate cell technology represents improvement in ASR and durability. This test completed 2000 hours of testing. The power degradation rate achieved was 0.78%/1000 hours, near the target of 0.75%/1000 (Figure 59). The test contained 4 strips with 4 different cathode technologies at half-strips distributed across the block (Figure 60). Performance was measured at ¼ strip level, so 2 ASR reported values for each half-strip. The average ASR degradation (mohm-cm^2/khrs) rates for the various cathodes included in the test were: epsilon (22.2 mohm-cm^2/khrs), epsilon plus (19.1 mohm-cm^2/khrs), EIS1 (16.6 mohm-cm^2/khrs) and EIS2 (9 mohm-cm^2/khrs).

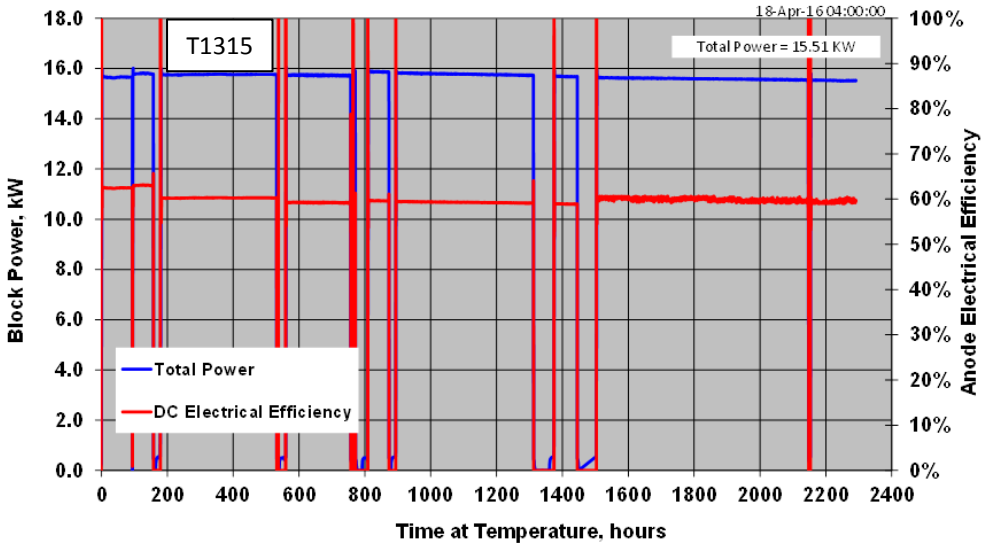

Figure 59. T1315 power and efficiency plot

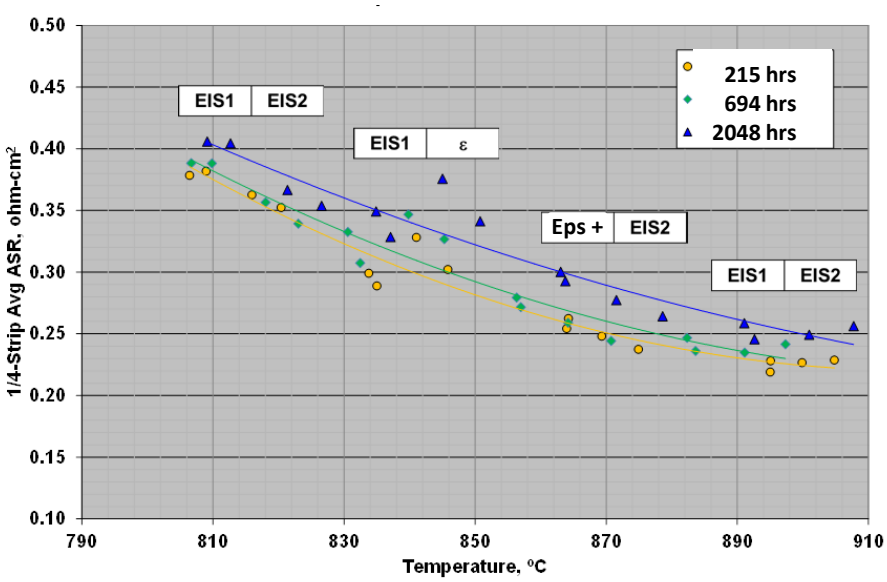

Figure 60. T1315 ASR versus temperature sweeps

Conclusions – Starting ASR levels for the block tests were as expected based on the subscale databases and support the assessment of current LGFCS stack technology at 0.28 ohm-cm^2. Based on subscale testing (Figure 34) ASR degradation rates are higher during the early stages of testing and reduced over time. These degradation rates are typical of the subscale tests. Block test rigs are being converted to accommodate the integrated block product designs (Figure 61). Longer durability testing of blocks of the product design and with finalized balance of plant components for complete TRL6 scale testing is proceeding at LGFCS.

Figure 61. Compact product block design (3 blocks shown) able to accommodate 6 versus 5 strips

Task 5.0 – Manufacturing

This task supports the cost of materials, substrate printing, strip assembly, strip electrochemical QA/performance testing and shipping of the strips necessary for the proposed block test. A minimum of 4 strips to achieve >15 kW will be produced.

Results and Discussion – The decision was made to utilize the same technology (epsilon cathode) present in the 220kW IST test for the additional SECA supported block test. The material cost of those strips was captured under this task.

This task supported the printing of full-scale tubes required for TRL5 level testing. These included:

1. As mentioned in the primary interconnect section, 63 cell substrates having a reduced primary interconnect dimension were successfully fabricated and tested, showing a 5.8% power increase. The reduced primary interconnect dimensions allowed the addition of 3 additional cells to the substrate.
2. A batch of full-scale substrates having a revised primary interconnect layer pattern and materials set was successfully printed that achieved a lower ASR. These substrates were of the standard 60-cell primary interconnect pitch

GRAPHICAL MATERIALS LIST

LIST OF ACRONYMS

ACC	Anode Current Collector
ASR	Area Specific Resistance
ATBT	Ambient Triple Bundle Test
BC	Button Cell
BM	Bundle Middle Condition
BOP	Balance of Plant
CA, CAT	Cathode
CCC	Cathode Current Collector
CIC	Ceramic Interconnector
CTE	Coefficient of Thermal Expansion
CWRU	Case Western Reserve University
DC	Direct Current
DL	Dense Layer
DOE	Department of Energy
EDS	Energy Dispersive Spectroscopy
EIS	Entry Into Service, Electrochemical Impedance Spectroscopy
ESD	Emergency Shutdown
ELE	Electrolyte
HC	High Current Density
IP	Integrated Planar
IST	Integrated String Test
LGFCS	LG Fuel Cell Systems
LNF	Lanthanum Nickel Ferrite
LSCF	Lanthanum Strontium Cobalt Ferrite
LSM	Lanthanum Strontium Manganese
MMA	Magnesia Magnesium Aluminate
NC	Normal Current Density
NG	Natural Gas
NOC	Normal Operation Condition
OCV	Open Circuit Potential
OGB	Off Gas Burner
PBC	Pressurized Button Cell
PBT	Pressurized Bundle Cell
PCT	Penta-Cell test
PIC	Primary Interconnect
PTT	Pressurized Tube Test
Rp	Polarization Resistance
RU	Repeat Unit
SECA	Solid State Energy Conversion Alliance
SLA	Single Layer Anode
SOFC	Solid Oxide Fuel Cell
TEM	Transmission Electron Microscope
TPB	Three Phase Boundary
TRL	Technology Readiness Level
TRT	Tube Run Test
UK	United Kingdom
WDS	Wavelength Dispersive Spectroscopy
XRD	X-ray Diffraction
YSZ	Yttria-Stabilized Zirconia